Journal of Glaciology

Article

Cite this article: Krabbendam M, Dioguardi F, Arnhardt C, Roberson S, Hall AM (2023). Drag forces at the ice-sheet bed and resistance of hard-rock obstacles: the physics of glacial ripping. *Journal of Glaciology* **69**(273), 103–119. https://doi.org/10.1017/jog.2022.49

Received: 23 December 2021
Revised: 27 May 2022
Accepted: 27 May 2022
First published online: 1 July 2022

Key words:
Glacier hydrology; processes and landforms of glacial erosion; subglacial processes; subglacial sediments

Author for correspondence:
M. Krabbendam, E-mail: mkrab@bgs.ac.uk

cambridge.org/jog

Drag forces at the ice-sheet bed and resistance of hard-rock obstacles: the physics of glacial ripping

Maarten Krabbendam[1], Fabio Dioguardi[1], Christian Arnhardt[2], Sam Roberson[3] and Adrian M. Hall[4,5]

[1]British Geological Survey, Lyell Centre, Edinburgh, UK; [2]British Geological Survey, Keyworth, Nottingham, UK; [3]Geological Survey of Northern Ireland, Belfast, Northern Ireland, UK; [4]Department of Physical Geography, University of Stockholm, Stockholm, Sweden and [5]Institute of Geography, University of Edinburgh, Edinburgh, UK

Abstract

Glacial ripping involves glaciotectonic disintegration of rock hills and extensive removal of rock at the ice-sheet bed, triggered by hydraulic jacking caused by fluctuating water pressures. Evidence from eastern Sweden shows that glacial ripping caused significant subglacial erosion during the final deglaciation of the Fennoscandian ice sheet, distinct from abrasion and plucking (quarrying). Here we analyse the ice drag forces exerted onto rock obstacles at the base of an ice sheet, and the resisting forces of such rock obstacles: glaciotectonic disintegration requires that ice drag forces exceed the resisting forces of the rock obstacle. We consider rock obstacles of different sizes, shapes and fracture patterns, informed by natural examples from eastern Sweden. Our analysis shows that limited overpressure events, unfavourable fracture patterns, low-transmissivity fractures, slow ice and streamlined rock hamper rock hill disintegration. Conversely, under fast ice flow and fluctuating water pressures, disintegration is possible if the rock hill contains subhorizontal, transmissive fractures. Rock steps on previously smooth, abraded surfaces, caused by hydraulic jacking, also enhance drag forces and can cause disintegration of a rock hill. Glacial ripping is a physically plausible erosion mechanism, under realistic glaciological conditions prevalent near ice margins.

Introduction

Ice-sheet beds on hard basement rocks below contemporaneous and past ice are commonly rough, with innumerous rock hills of various shapes and sizes (Roberts and Long, 2005; Krabbendam and Bradwell, 2014; Lindbäck and Pettersson, 2015; Cooper and others, 2019). Here we examine the balance of resisting and ice drag forces that act on such rock hills and consider how the entry of pressurised meltwater into rock fractures changes the balance of these forces. This problem is relevant to subglacial erosion processes. Abrasion and plucking (quarrying) are generally seen as the main mechanisms of subglacial erosion, with subglacial fluvial erosion locally important (e.g. Glasser and Bennett, 2004; Alley and others, 2019). Recently, a further effective subglacial erosion mechanism, *glacial ripping*, has been recognised to have operated in eastern Sweden (Hall and others, 2020; Krabbendam and others, 2022), NW Scotland (Hall and others, 2021) and possibly eastern Canada (Bukhari and others, 2021), below Pleistocene ice sheets that covered these areas. Glacial ripping can remove large parts or all of a rock hill such as a roche moutonnée (Hall and others, 2020; Krabbendam and others, 2022). The process is considered to involve three steps (Fig. 1): (1) hydraulic jacking caused by overpressure of subglacial meltwater entering fractures in the shallow rock mass; (2) glaciotectonic disintegration of rock hills and (3) transport of boulders and deposition as boulder spreads or immature rubble till. Glacial ripping is a 'mass' event, involving hundreds to thousands of blocks at more or less the same time, and affecting a large part or the entirety of a rock hill, distinct from classic lee side plucking, which only removes rock one block at a time (Krabbendam and others, 2022). While there is good field evidence (summarised below) to support this three-stage mass process (Hall and others, 2020, 2021; Krabbendam and others, 2021, 2022), the theoretical understanding of the process is still limited.

Here we explore the theoretical basis of the glaciotectonic disintegration of rock hills, subjected to high water pressure events and resultant hydraulic jacking occurring at the ice bed. In the conceptual model it is envisaged that (transient) high pressure water at the ice bed penetrates into fractures in the bedrock below (Hall and others, 2020; Krabbendam and others, 2021, 2022). This lowers the static friction along these fractures and, if the water pressure in the fracture exceeds the overburden pressure of overlying ice and rock, it leads to hydraulic jacking. Hydraulic jacking in turn results in loss of rock mass strength and local brecciation of the rock hill in question. It may also locally displace blocks upwards, creating sharp edges on the previously smooth, abraded ice bed (Forssberg and others, 2007; Krabbendam and others, 2022). Continuing application of ice drag forces then further disintegrates the rock hill.

At issue is whether the resisting forces of the rock hill or rock obstacle are sufficiently lowered so that the ice drag forces exceed them, allowing disintegration of the rock mass. To

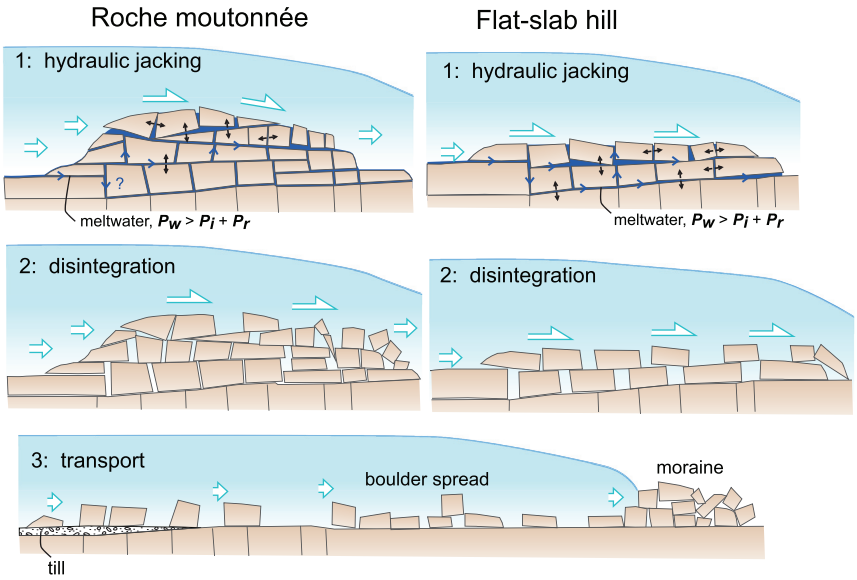

Fig. 1. Conceptual model for glacial ripping as a three-stage subglacial erosion mechanism – after Hall and others (2020). Figure © Svensk Kärnbränslehantering. Reproduced with permission.

address this issue we model: (1) the drag forces exerted by ice creeping past rock obstacles of variable size and shape at the base of an ice sheet; and (2) the resisting forces of rock obstacles with variable size, shape and internal fracture network configurations; and how these forces are affected by high water pressure events. The scenarios are modelled as a function of glaciological variables such as basal water pressure and ice velocity, and geological/topographical variables such as fracture patterns and obstacle size. We then assess the force balance and assume that block movement, and hence glacial ripping, can occur if the drag forces exceed the resisting forces. We thus test if glacial ripping is a physically plausible process, and under what glaciological and geological conditions it may, or may not, operate at the base of an ice sheet.

Setting and summary of field evidence

We base our modelling on examples of glacial ripping in basement gneisses in eastern Sweden (Hall and others, 2020; Krabbendam and others, 2022), below the retreating Late Weichselian Fennoscandian ice sheet (FIS). The bedrock in the region consists of crystalline basement ('shield rock'), with variable fracture patterns and fracture spacing, the latter varying from <0.2 to over 5 m (Jern, 2004; Krabbendam and others, 2021). Locally, long subhorizontal fractures occur in the shallow (<10 m) bedrock; elsewhere rocks are more massive, or vertical fractures dominate over subhorizontal ones (e.g. Carlsson, 1979; Goodfellow and others, 2019; Krabbendam and others, 2021). In the near-surface bedrock, horizontal stresses are greater than vertical stresses, and these tend to hold vertical fractures tight (Glamheden and others, 2007; Hökmark and Lönnqvist, 2014), so that the prevailing stress field favours dilation and hydraulic jacking of shallow horizontal fractures.

Fennoscandia was repeatedly glaciated by ice sheets throughout the Pleistocene. The last FIS, with a maximum ice thickness of 3000–3500 m (Quiquet and others, 2016), retreated rapidly between *c.* 15 and 10 ka over eastern Sweden, with a pause during the Younger Dryas. In east central Sweden, ice margin retreat was by calving in a shallow lacustrine or marine setting (Lundqvist, 1987; Andrén and others, 2011), with retreat rates estimated at 300–350 m a^{-1} (Strömberg, 1989; Stroeven and others, 2016). Mapping of shorelines, combined with accurate varve chronology, suggests that sea or lake level during the deglaciation of east central Sweden was ~150–190 m higher than present sea level, implying a significant water depth at the retreating calving margin (Hedenström and Risberg, 2003; Johnson and others, 2010).

Large areas of lowland Sweden show typical landscapes of glacial erosion developed in gneissic basement rocks with abundant whalebacks and roches moutonnées (Hall and others, 2019). Over substantial areas such rock hills have been disintegrated by a process interpreted to be glacial ripping (Hall and others, 2020). Field evidence for glacial ripping comprises three components (after Hall and others, 2020; Krabbendam and others, 2021; Krabbendam and others, 2022):

(1) Dilated subhorizontal fractures, locally sediment-filled, indicating hydraulic jacking, affecting the upper 1–13 m of bedrock (Fig. 2a). This includes cases where rock steps were formed on the previously smooth rock surfaces by differential uplift of fracture-bound rock blocks in the substrate (Fig. 2b).
(2) Partially disintegrated rock hills, such as roches moutonnées (Fig. 2c), in which fractures have been dilated, voids and caves have opened, with extensive evidence of block displacement and removal (Fig. 2d). This disintegration typically increases down-ice, but may affect the entire rock hill, involving hundreds of blocks.
(3) Extensive (thousands of square metres) occurrence of boulder spreads; fields of large (1–5 m) angular boulders, normally of the same lithology, with a spatial density of boulders that far exceeds those normally seen in a basement terrain subjected to glacial plucking (Fig. 2e). The boulders have been transported and dispersed subglacially, but with small transport distances, typically <1 km (Fig. 2f), consistent with limited edge rounding.

Modelling approach

Background and assumptions

A complex process such as glacial ripping is influenced by a wide range of parameters, each with a range of possible values. To focus our modelling, this range of parameters needs to be restricted: some parameters are not explicitly modelled, but are discussed. Field evidence suggests that damage from glacial ripping was particularly effective below the ablation zone, close to the retreating margin of the Pleistocene ice sheets, and thus constituted an intensive phase of subglacial erosion just prior to deglaciation (Hall and others, 2020, 2021; Bukhari and others, 2021; Krabbendam and others, 2021, 2022). We thus focus on glaciological conditions beneath the last FIS during its late stage of

https://doi.org/10.1017/jog.2022.49 Published online by Cambridge University Press

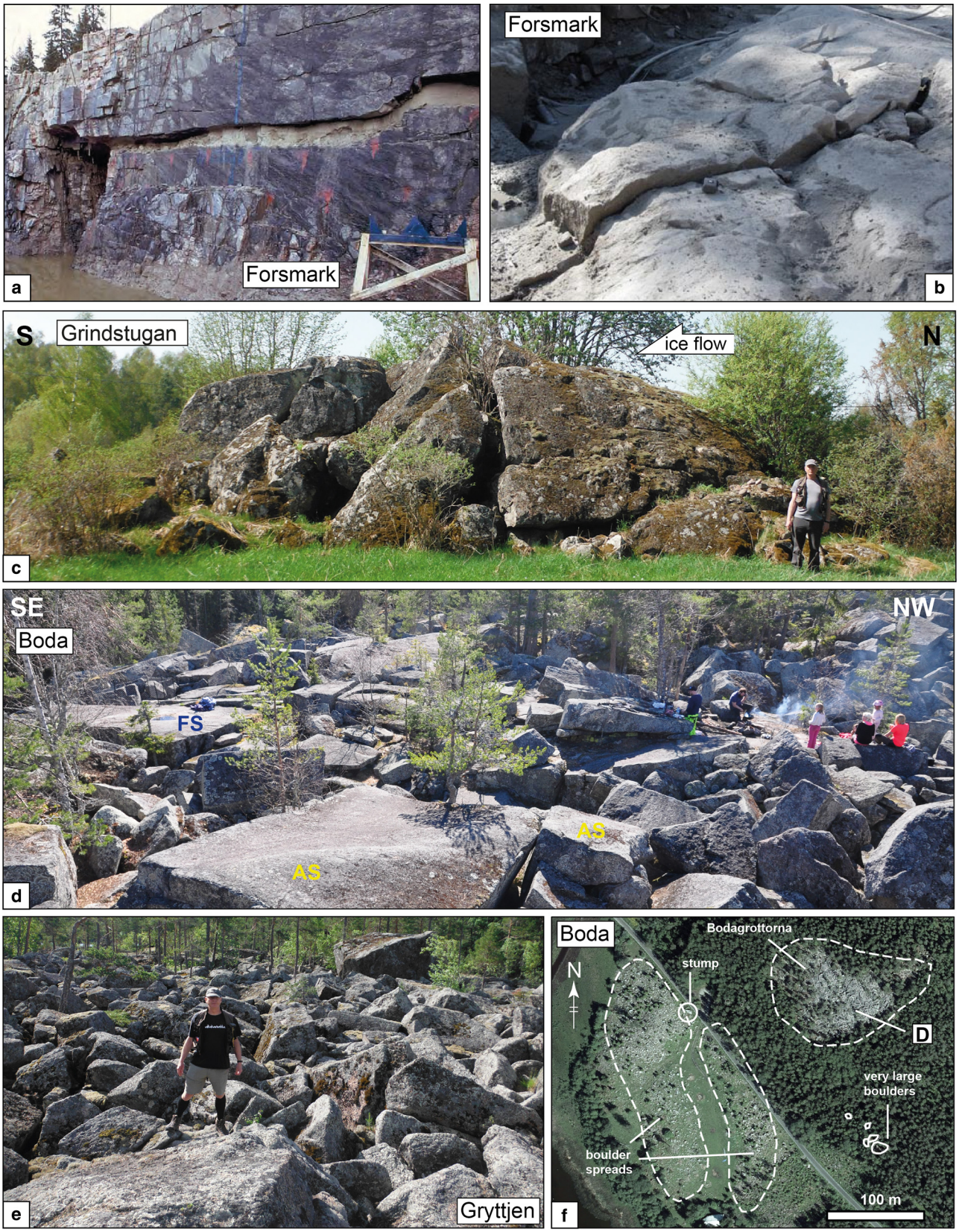

Fig. 2. Field evidence for glacial ripping in eastern Sweden. (a) Dilated, jacked subhorizontal fracture (50 cm high) with sediment-fill in construction excavation, Forsmark nuclear power plant (Leijon, 2005; Figs 5-1). Photo: Göran Hansson. (b) Upward jacked block with rock step, disrupting the abraded surface; temporary excavation AFM 001364, Forsmark (Forssberg and others, 2007; fig. B5). (c) Small disintegrated roche moutonnée near Grindstugan, Uppsala county. (d) Part of top surface of the large, partially disintegrated roche moutonnée of Bodagrottorna, Gävleborg county. (e) Boulder spread of angular boulders. Gryttjen, Gävleborg county. (f) Aerial photo (© Lantmäteriet) of two small boulder spreads, showing <250 m transport in an SSE direction. Bodagrottorna disintegrated roche moutonnée to the NE. Figure © Svensk Kärnbränslehantering. Reproduced with permission.

https://doi.org/10.1017/jog.2022.49 Published online by Cambridge University Press

final deglaciation. Direct glaciological controls exerted by this palaeo-ice sheet are evidently not available, but the Greenland ice sheet (GrIS) is also in a state of retreat, so we use observations from the ablation zone of the GrIS as an analogue for the retreating Pleistocene ice sheets.

Relevant assumptions are as follows:

(1) *Basal thermal regime*. The ice-sheet bed was 'warm' or thawed. Abundant abraded surfaces decorated with striae show that abrasion (and hence warm-based sliding) was active prior to deglaciation in eastern Sweden (e.g. Sohlenius and others, 2004); ice-sheet models also simulate warm-based conditions close to the retreating margin (e.g. Näslund and others, 2003; Patton and others, 2017). Similarly, the base of the GrIS ablation zone is thawed (Macgregor and others, 2016), and ice motion shows a significant component (45–75%) of basal sliding (Ryser and others, 2014).

(2) *Ice viscosity*. We model ice as a viscous Newtonian medium, with the viscosity as established experimentally by Byers and others (2012). This makes the treatment simpler (see also Nye, 1970; Hallet, 1979), but is also realistic for temperate ice (Colbeck and Evans, 1973; Chandler and others, 2008; Byers and others, 2012; Krabbendam, 2016). In essence, we thus assume a layer of temperate ice, thicker than the highest rock obstacles. In Greenland, borehole temperature measurements show a 30–100 m thick basal layer of temperate ice at 20–50 km from the margin, whereas close to the margin the entire ice thickness is temperate (Lüthi and others, 2002; Ryser and others, 2014; Harrington and others, 2015; Harper and others, 2019). The effects of cold ice, with its different rheological behaviour, is discussed but not modelled.

(3) *Ice sliding velocity*. Patton and others (2017) modelled maximum ice surface velocities of 200–400 m a^{-1} during the deglaciation of eastern Sweden. In the GrIS ablation zone, basal sliding velocities are *c.* 50–75% of the surface velocities (Ryser and others, 2014), so we assume a value of ~300 m a^{-1} as a maximum realistic sliding velocity.

(4) *Ice thickness*. Although the FIS reached a maximum thickness of *c.* 3000 m during late glacial maximum conditions (Quiquet and others, 2016), field evidence suggests that glacial ripping was particularly active just prior to deglaciation, hence with low ice thickness. In the lower ground in eastern Sweden, ice retreat was dominated by calving in the Baltic Ice Lake, with water depth up to 180 m. We assume an ice thickness of 300 or 600 m.

(5) *Basal water pressure fluctuations*. Evidence for hydraulic jacking includes dilated and sediment-filled fractures (see section 'Setting and summary of field evidence'). High water pressures, including overpressure when temporarily exceeding overburden pressure (P_i), have been measured or demonstrated at the base of the GrIS ablation zone in the following settings. Firstly, dramatic supraglacial lake drainage events can lift up the ice surface over several square kilometres (Das and others, 2008; Doyle and others, 2013) and these represent high-magnitude overpressure events, involving volumes >10^6 m^3 water, resulting in substantial ice–bed separation. Secondly, high-frequency (daily in the melt season), but short-lived (hours), water-pressure fluctuations between 80 and 110% of P_i have been measured in boreholes (Andrews and others, 2014; Claesson Liljedahl and others, 2016; Wright and others, 2016; Harper and others, 2019). The long-term average water pressure in these boreholes is *c.* 90–95% of P_i, although some boreholes show long-term close to or exceeding 100% of P_i. These water pressure fluctuations are highly localised events (out-of-phase with adjacent boreholes) and thus represent low-magnitude events, involving only small volumes of water, with only localised ice–bed separation. However, they occur repeatedly (tens of times) throughout the melting season. Thirdly, Andrews and others (2014) noticed an additional setting, where moulins are well-connected to the glacier bed, preventing overpressure to build up. In this regime, frequent water pressure fluctuations occur between 60 and 98% of P_i, with a long-term average of *c.* 80% of P_i. All three processes are likely to have occurred during deglaciation of the FIS and may have led locally to hydraulic jacking in eastern Sweden. Thus, for modelling purposes we assume that high water pressure events, including overpressure events, occurred at the ice bed near and around the idealised obstacles under discussion. We do not model or discuss the specific dynamics or spatial extent of high water-pressure events in Sweden. We further assume that the normal stress at the ice bed equals the overburden pressure of the ice.

(6) We make the simplifying assumption that the fracture patterns of the bedrock are broadly orthogonal, and dominated by subhorizontal and subvertical fractures. Such patterns are common in basement rocks in Sweden and elsewhere (Talbot and Sirat, 2001; DeWandel and others, 2006; Pless and others, 2015; Krabbendam and others, 2021), and near ubiquitous in flat-lying sedimentary rocks. However, we do model two different fracture patterns: (a) a scenario where all fractures are continuous in-plane, and (b) a scenario where subhorizontal fractures occur at different levels ('stepped') but joined to subvertical fractures, via T-junctions, thus being discontinuous in a single plane. This is similar to the 'step-path' failure mechanisms recognised in large rock-slope failures (e.g. Brideau and others, 2009). In-plane rock bridges along a single fracture (Kemeny, 2003; Hooyer and others, 2012; Elmo and others, 2018), and parts of the fracture sealed by fracture fills (Shang and others, 2016), also represent discontinuous fractures and may hamper hydraulic jacking. During overpressure events in which hydraulic jacking occurred, some rock bridges were likely broken by hydraulic fracturing, forming longer, more continuous fractures.

Modelling scenarios

The geometry of the ripped bedrock hills, their internal fracture networks and the resultant effects of glacial ripping in eastern Sweden are highly variable. We confine ourselves to model a number of simple scenarios, informed by natural examples, but including some end-member scenarios (Figs 3a–e):

(1) a blunt hemispherical obstacle of intact rock, without a basal fracture;
(2) a blunt hemispherical obstacle with a continuous, subhorizontal basal fracture;
(3) a blunt hemispherical obstacle with a discontinuous basal fracture, formed by steps in the basal fracture system;
(4) an elongate obstacle with subhorizontal fractures and a blunt stoss side, but a large flat top;
(5) a small rock step, caused by the differential uplift of a rock block, which then protrudes above the surrounding rock surface. This scenario is applicable to the smooth, abraded top surfaces of large hills and low relief rock surfaces.

The basis of the modelling is the principle that if the drag force F_d exerted by ice flowing past a blunt obstacle exceeds the resisting forces F_r of that obstacle, then the obstacle moves or disintegrates:

$$F_d > F_r \quad (1)$$

All variables and constants are also shown in Table 1.

https://doi.org/10.1017/jog.2022.49 Published online by Cambridge University Press

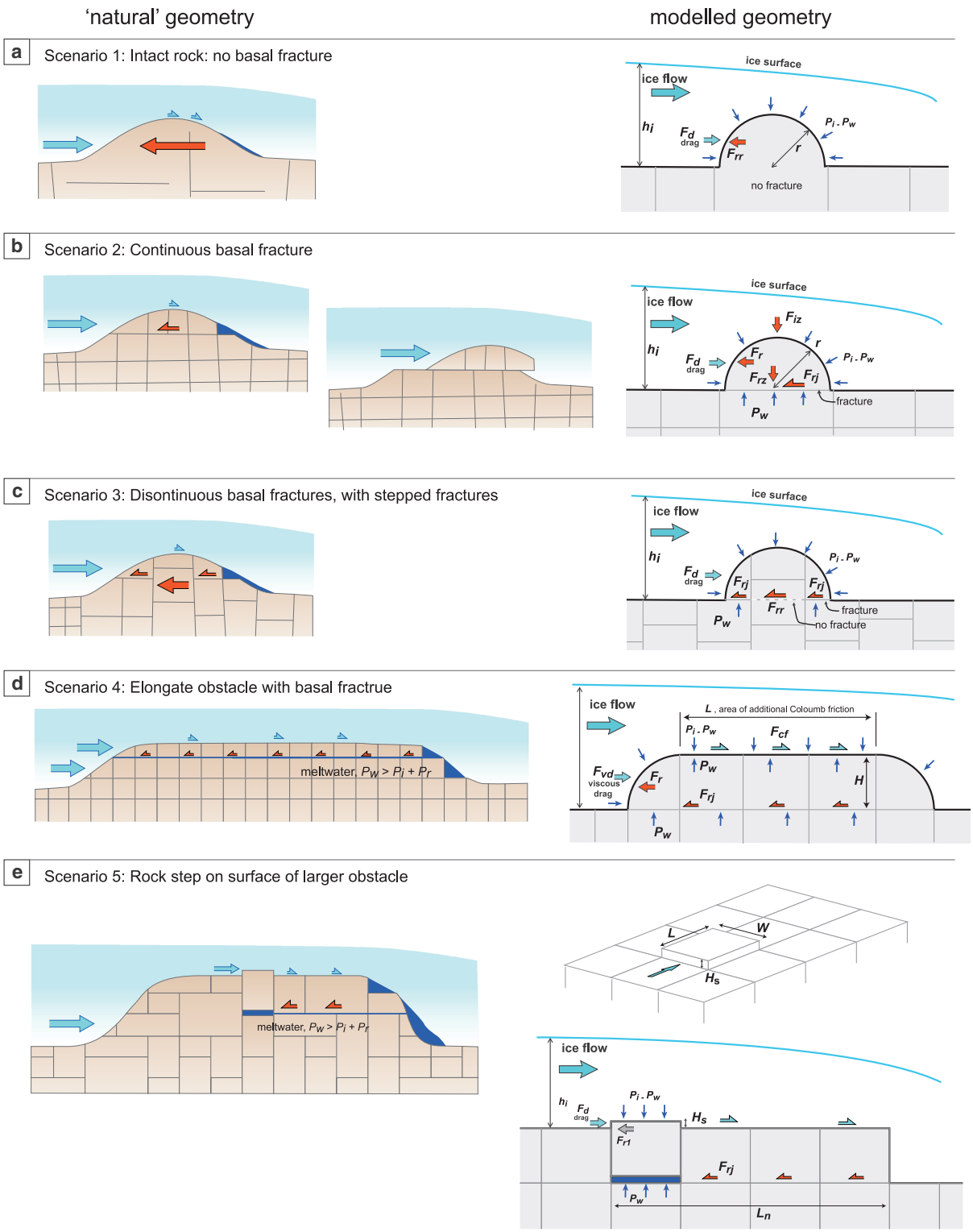

Fig. 3. Modelling scenarios 1–5: conceptual geometries; modelled geometries with some parameters indicated – see also Table 1. Figure © Svensk Kärnbränslehantering. Reproduced with permission.

Drag forces for a hemispherical obstacle

Temperate ice is modelled as a viscous Newtonian medium creeping at low velocities (Hallet, 1979; Byers and others, 2012). In this laminar flow regime with very low Reynolds number ($Re \ll 1$), also known as Stokes regime, the drag force F_d on a spherical particle has been obtained by solving the Navier–Stokes equations (Stokes, 1951; Loth, 2008):

$$F_d = 6\pi\eta U r \tag{2}$$

where η is the viscosity, U the velocity of the medium and r the radius of a spherical particle. F_d is a combination of form drag, which depends on the shape of the particle because it arises from the pressure the fluid exerts on the cross-sectional area of the object perpendicular to the streamlines, and viscous friction (skin) drag, which is due to the tangential shear stress at the particle surface (Leith, 1987). In a normal viscous medium, the creep velocity right at the contact is zero (non-slip boundary), and the tangential shear stress at the obstacle surface is substantial. This is patently not the case for a thawed ice–bed contact, where sliding

https://doi.org/10.1017/jog.2022.49 Published online by Cambridge University Press

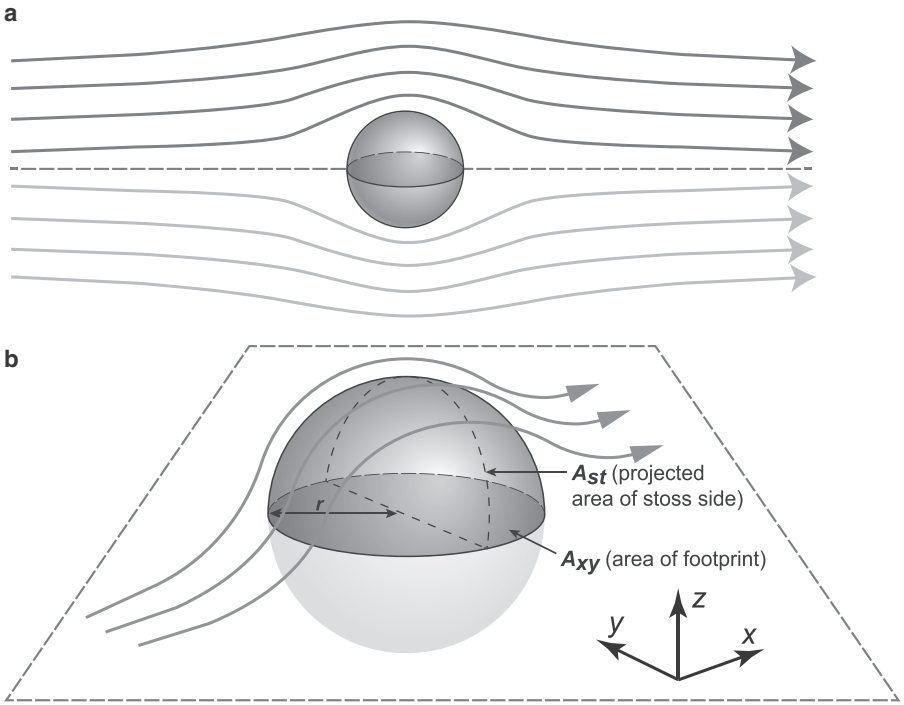

Fig. 4. Principle of applying Stokes law for laminar flow around a sphere to a hemispherical obstacle: (a) laminar flow around a sphere and (b) hemispherical obstacle, in a half space, within a laminar flow field. Area of projected stoss side A_{st} and area of footprint of obstacle A_{xy} are indicated. Direction of ice flow = x. Figure © Svensk Kärnbränslehantering. Reproduced with permission.

is known to occur with a thin film of water between the obstacle and the ice. Thus, for temperate ice creeping past an obstacle, skin drag may be low. For this reason, some authors suggest that $F_d = 4\pi\eta Ur$ (e.g. Hallet, 1979; Cohen and others, 2005). However, Byers and others (2012) empirically confirmed that Eqn (2) is broadly valid (with values for the numerical prefactor of 5.5π; 6.9π and 7.5π) for temperate ice. Since we also use the experimental values of ice viscosity from the same experiments (see above), we herein use Eqn (2) as is. However, we cut the sphere in half to model a hemispherical obstacle (Fig. 4) so that:

$$F_d = 3\pi\eta Ur \tag{3}$$

We ignore the effects of regelation because the large size of the rock obstacles compared to smaller debris particles diminishes the heat flow effect through the obstacle and thus renders regelation inefficient over length scales greater than a few centimetres (see also Hallet, 1979; Cuffey and Patterson, 2010; Byers and others, 2012).

Note that the 'sliding laws' as derived by for instance by Nye (1970; see discussion in Cuffey and Patterson, 2010), are broadly similar in concept, except that these sliding laws integrate obstacle size over a number of obstacles and thus employ a roughness parameter rather than the size of an individual obstacle, and use the overall basal shear stress, rather than the force exerted on an individual obstacle.

Drag forces for a non-hemispherical, elongate obstacle

Viscous drag forces for a non-hemispherical obstacle are more complicated since they depend on the shape of the object, which needs to be quantified with a shape descriptor, which treats the form and skin drag separately (e.g. Leith, 1987; Ganser, 1993; Bagheri and Bonadonna, 2016; Dioguardi and others, 2018). These approaches all assume a non-slip boundary, and thus are not appropriate in our case, because there is certainly slip along a thawed ice–bed contact. To approximate the drag forces on elongate obstacles, we model a geometry where we split the obstacle in (1) a blunt stoss side that faces ice flow, and (2) a flat horizontal top surface parallel to ice flow (Fig. 3d). We assume that (1) the drag force F_{vd} at the stoss side is controlled by the viscous drag acting upon that stoss face (with surface A_{st}) and controlled by a form of Stokes law and that (2) the drag forces F_{cf} on the flat top surface area are controlled by a simple friction law acting on the top surface (with surface A_{xy}). This ice–rock friction is complex in detail, and different from normal rock–rock friction, because of the presence of rock debris particles between the ice and the bed, variations in concentration and particle size of the debris at the ice bed, and ice deformation and melting around the particles (Hallet, 1979; Emerson and Rempel, 2007; see also discussion in Schweizer and Iken, 1992). Nevertheless, integrated over a large area, the concept of bulk Coulomb friction appears to be valid (Cohen and others, 2005; Emerson and Rempel, 2007; McCarthy and others, 2017), and is used herein:

$$F_{cf} = \mu_{ir}\, F_{iz} \tag{4}$$

where μ_{ir} is the bulk friction coefficient on the ice–rock contact. We take μ_{ir} at 0.05, at the lower end of experimentally obtained values (from Cohen and others, 2005; Emerson and Rempel, 2007; McCarthy and others, 2017); effects of higher friction coefficients as measured by Emerson and Rempel (2007) are not modelled but will be discussed. The normal force F_{iz} exerted by the overlying ice is a function of thickness and density of ice (cryostatic pressure P_i), the water pressure P_w and the horizontal surface area A_{xy} over which it operates as follows:

$$F_{iz} = (P_i - P_w)\, A_{xy} \tag{5}$$

The horizontal surface A_{xy} is approximately equal to the surface area of the basal fracture of the rock obstacle. As we wish to explore the effects of relative overpressure P_w/P_i

https://doi.org/10.1017/jog.2022.49 Published online by Cambridge University Press

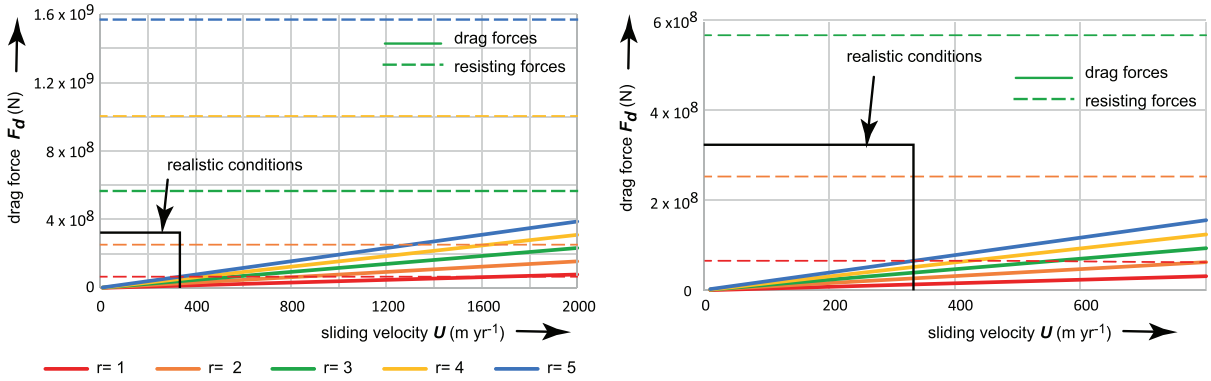

Fig. 5. Drag forces F_d (solid lines) and resisting forces F_r (dashed lines) as a function of sliding velocity U, for a hemispherical obstacle without basal fracture, for obstacles with radii 1–5 m; Eqns (3) and (11). Intact rock strength τ_r taken at 20 MPa. Figure © Svensk Kärnbränslehantering. Reproduced with permission.

Table 1. Variables, constants and parameters used

Variable	Description	Range	Unit	Reference/comment
F_d	Total drag force exerted on a rock hill		N	
F_r	Total resisting forces of a rock hill		N	
F_{cf}	Friction force (on flat surfaces only)		N	
F_{rr}	Resisting force by intact rock		N	
F_{rj}	Frictional resisting force along a rock–rock fracture		N	
F_{iz}	Normal force exerted by overlying ice		N	
F_{rz}	Normal force acting on a horizontal fracture		N	
F_{bz}	Buoyant weight of the block		N	
F_{vd}	Viscous drag force acting on stoss side		N	
P_i	Overburden pressure (of ice and rock)		Pa	
P_w	Water pressure		Pa	
r	Radius of hemispherical obstacle	0–10	m	
U	Basal sliding velocity of ice	0–300	m a^{-1}	In modelling calculated as m s^{-1}
A_{st}	Projected surface area of the stoss side (a vertical surface)		m^2	
A_{xy}	Surface area of the basal footprint of the obstacle (a horizontal surface)		m^2	
A_j	Surface area of the basal footprint of the obstacle, occupied by a fracture (a horizontal surface)		m^2	
A_r	Surface area of the basal footprint of the obstacle, occupied by intact rock (a horizontal surface)		m^2	
W, H, L	Width, height and length of obstacle		m	
L_n	Cumulative length of blocks down-ice from rock step (see Fig. 3e)		m	
T_j	Transmissivity factor	0–1	–	
Constant/ parameter	Description	Value or range	Unit	Reference/comment
g	Gravitational constant	9.8	m s^{-2}	
η	Viscosity of creeping medium (temperate ice)	1.3×10^{11}	Pa s	Byers and others (2012)
μ_{ir}	Friction coefficient on ice–rock contact (i.e. along the ice bed)	0.05	–	Cohen and others (2005); Emerson and Rempel (2007) report a range of *c.* 0.01–0.3
μ_{rr}	Friction coefficient on rock–rock contact (i.e. along a fracture)	0.7	–	Ramana and Gogte (1989) report a range of 0.64–0.77; Glamheden and others (2007) report a range of 0.48–0.77, with a mean of 0.67
τ_r	Shear strength of intact rock	20	MPa	Singh and others (2017) report a range of 10–35 MPa
h_i	Ice thickness	300 or 600	m	
ρ_i	Density of ice	910	kg m^{-3}	
ρ_r	Density of rock	2800	kg m^{-3}	

(in essence the potential effects of hydraulic jacking), this is rewritten as:

$$F_{iz} = gh_i\rho_i\left(1 - \frac{P_w}{P_i}\right)A_{xy} \quad (6)$$

where g is the gravitational constant, h_i the ice thickness and ρ_i the density of ice. Total friction on the flat surfaces then becomes:

$$F_{cf} = \mu_{ir}\, gh_i\rho_i\left(1 - \frac{P_w}{P_i}\right)A_{xy} \quad (7)$$

Note that Coulomb friction F_{cf} will approach zero if P_w approaches P_i; since a frictional force cannot be negative, Eqns (5)–(7) are thus only valid for $P_w \leq P_i$.

The viscous drag F_{vd} acting on the stoss side can be approximated by assuming that it is controlled by the square root of the

https://doi.org/10.1017/jog.2022.49 Published online by Cambridge University Press

vertical surface area that faces up-ice (the projected 'stoss-side surface area' A_{st}, which is half the surface area of a circle with radius r, or the width W multiplied by height H for a rectangular obstacle):

$$A_{st} = \frac{1}{2}\pi r^2 \quad \text{so that} \quad r = \sqrt{2\,A_{st}/\pi} \tag{8}$$

The viscous drag component then becomes ((3) combined with (8)):

$$F_{vd} = 3\,\eta U\sqrt{2A_{st}/\pi} \tag{9}$$

The total drag forces of a non-hemispherical obstacle is then ((7) and (9)):

$$F_d = 3\eta U\sqrt{2\,A_{st}/\pi} + \mu_{ir} g h_i \rho_i \left(1 - \frac{P_w}{P_i}\right) A_{xy} \tag{10a}$$

For a rectangular cuboid-shaped obstacle, with width W, height H and length L this becomes:

$$F_d = 3\,\eta U\sqrt{2HW/\pi} + \mu_{ir} g h_i \rho_i \left(1 - \frac{P_w}{P_i}\right) WL \tag{10b}$$

Resisting forces for a hemispherical obstacle without fractures

If the rock obstacle is poorly fractured, for instance if the rock hill is smaller than the vertical fracture spacing in the local bedrock, or if no continuous subhorizontal fractures are present (Fig. 3a), the resisting force of intact rock F_{rr} is controlled by the intact rock strength as follows:

$$F_{rr} = \tau_r A_r \tag{11}$$

where τ_r is the shear strength of intact rock, and A_r the surface area of the potential shear plane of the intact rock. Shear strength values for intact rock are rarely measured, in contrast to uniaxial compressive strength (UCS) and tensile strength. Singh and others (2017) obtained shear strength of between *c.* 10 and 35 MPa for different gneisses. Shear strength is typically 20–30% of UCS, and about twice the tensile strength. Rock mechanic tests on rocks near Forsmark yielded a range of 160–370 MPa for UCS and 10–18 MPa for tensile strength (Glamheden and others, 2007), suggesting shear strength range of 20–60 MPa. We take a conservative value of ~20 MPa for τ_r, as in nature rocks may contain micro-structures, which lower the shear strength.

Resisting forces for a hemispherical obstacle with continuous basal fracture

If a rock hill contains fractures – as most do – its rock mass strength is lower than that of intact rock. Rock mass strength is complex, so we consider the simple scenario of an obstacle with a single continuous subhorizontal fracture at its base (Fig. 3b). The resisting force F_{rj} along this fracture can be defined by:

$$F_{rj} = \mu_{rr} F_{rz} \tag{12}$$

where μ_{rr} is rock–rock friction coefficient along the basal fracture, and F_{rz} the normal force acting on the basal fracture. Rock–rock friction coefficient concerns the sliding of two rock blocks along a fracture (different from the ice–rock friction discussed previously) and varies with rock type and fracture roughness; for natural fractures in gneissic rocks Ramana and Gogte (1989) report a range of 0.64–0.77; Glamheden and others (2007) report a range of 0.48–0.77, with a mean of 0.67, for rocks at Forsmark. We take a value of 0.7. We ignore fracture cohesion, since hydraulic jacking will have broken any such cohesion.

The normal force F_{rz} has two components:

$$F_{rz} = F_{bz} + F_{iz} \tag{13}$$

where F_{bz} is the buoyant weight of the rock above the fracture and F_{iz} is any force (weight) exerted by the overlying ice (as per Eqn (6)). The drag force exerted by ice flowing vertically downwards due to basal melting is ignored: while it is potentially important for small (centimetre-sized) debris particles under conditions of fast basal melting (Cohen and others, 2005; Byers and others, 2012), it becomes very small for metre-sized obstacles (Krabbendam and Hall, 2019).

The buoyant weight of the block is:

$$F_{bz} = V\,(\rho_r - \rho_w)g \tag{14}$$

where V is the volume of the block, ρ_r the density of rock and ρ_w the density of water. The total resisting force is then (Eqns (13), (14) and (6)):

$$F_{rj} = \mu_{rr}\left[V\,(\rho_r - \rho_w)g + g h_i \rho_i \left(1 - \frac{P_w}{P_i}\right) A_{xy}\right] \tag{15a}$$

For a hemispherical obstacle, as a direct function of r (with $V = (2/3)\pi r^3$ and $A_{xy} = \pi r^2$), this becomes:

$$F_{rj} = \mu_{rr}\left[\frac{2}{3}\pi r^3(\rho_r - \rho_w)g + g h_i \rho_i \left(1 - \frac{P_w}{P_i}\right)\pi r^2\right] \tag{15b}$$

For a rectangular cuboid-shaped obstacle, with width W, height H and length L, this becomes:

$$F_{rj} = \mu_{rr}\left[H\,W\,L\,(\rho_r - \rho_w)g + g h_i \rho_i \left(1 - \frac{P_w}{P_i}\right) WL\right] \tag{15c}$$

Effect of variable transmissivity of basal fractures

Thus far, it is assumed that the water pressure within a basal fracture equalises instantaneously with pressure fluctuations at the ice–bed contact, and leads to hydraulic jacking if relative overpressure P_w/P_i, exceeds 1, but this only happens if the fracture is highly transmissive (in the hydrological sense). Fracture transmissivity, however, is extremely variable in nature. Low transmissive fractures, for instance tight fractures or fracture planes with many rock bridges, would dampen the fluctuating water pressures in the fracture, and hence lower the peak water pressures within the fracture (e.g. Neupane and others, 2020). The water pressure in such fractures will remain close to the long-term average (e.g. 80–95% of P_i, depending on the long-term glaciohydrology of the relevant sector in the ice sheet) but not rise above 100%, and thus not cause hydraulic jacking. Fracture transmissivity can vary in nature easily by many orders of magnitude. Instead, we introduce dimensionless transmissivity factor T_j to model the effects of variable transmissivity along basal fractures, shown here for a hemispherical obstacle (Eqn (15b)):

$$F_{rj} = \mu_{rr}\left[\frac{2}{3}\pi r^3\,(\rho_r - \rho_w)g + g h_i \rho_i \left(1 - \frac{T_j\,P_w}{P_i}\right)\pi r^2\right] \tag{16}$$

https://doi.org/10.1017/jog.2022.49 Published online by Cambridge University Press

Resisting forces with discontinuous basal fracture and some intact rock

Fracture networks in the basement rocks of eastern Sweden (and elsewhere) are highly variable, and continuous subhorizontal fractures at the base of an obstacle are not ubiquitous: in various quarries and natural outcrops it was observed that subhorizontal fractures occur at different levels and are hence discontinuous (or: 'stepped'); in other sections subvertical fractures are dominant over subhorizontal fractures (Krabbendam and others, 2021). This variability is modelled as a hemispherical obstacle where the base constitutes part intact rock and part fracture (Fig. 3c). The total resisting force F_r is then the resisting force of the fracture plus that of intact rock, proportional to the area occupied by the basal fracture A_j and intact rock A_r respectively:

$$A_{xy} = A_r + A_j \quad and \; F_r = F_{rr} + F_{rj} \tag{17}$$

In proportion to area, this becomes:

$$F_r = F_{rr}\, A_r + F_{rj}\, A_j = F_{rr}\, A_{xy}\, \frac{A_r}{A_{xy}} + F_{rj} A_{xy}\, \frac{A_j}{A_{xy}} \tag{18}$$

So that, using Eqns (10) and (14):

$$F_r = A_{xy}\, \tau_{rk}\, \frac{A_r}{A_{xy}} + \frac{A_j}{A_{xy}}\, \mu_{rr} \left[V\, (\rho_r - \rho_w)g + g h_i \rho_i \left(1 - \frac{P_w}{P_i}\right) A_{xy} \right] \tag{19a}$$

and hence for a hemispherical obstacle:

$$F_r = \pi r^2 \tau_{rock}\, \frac{A_r}{A_{xy}} + \frac{A_j}{A_{xy}} \mu_{rr} \left[\frac{2}{3} \pi r^3\, (\rho_r - \rho_w)g + g h_i \rho_i \left(1 - \frac{P_w}{P_i}\right) \pi r^2 \right] \tag{19b}$$

Results

Different scenarios are calculated below and interpreted. For each scenario, both drag and resisting forces are calculated. Lines where drag force equals resisting force ($F_d = F_r$) are plotted for different obstacle radii as a function of ice sliding velocity and relative water pressure. Above the line, $F_d > F_r$ and the obstacle may be moved or disintegrated by the ice; below the line $F_d < F_r$ so one would expect the obstacle to remain in place.

On all relevant graphs (Fig 5-11), boxes with plausible glaciological conditions are indicated. These are constrained as water pressure varying between 60 and 105%, as measured below the GrIS (Andrews and others, 2014; Claesson Liljedahl and others, 2016; Wright and others, 2016), and maximum sliding velocities of 300 m a^{-1}.

Scenario 1: hemispherical obstacle without fractures

In hemispherical obstacles without basal fractures (Fig. 3a), the drag force F_d increases linearly with sliding speed U (Eqn (3)), whereas the resisting force F_r is constrained by the intact rock strength, independent of any glaciological parameter (Eqn (11)). The resisting forces generally exceed the drag forces, even for very high sliding velocities (Fig. 5). Small obstacles may fail at very high sliding velocities (>1700 m a^{-1}), velocities that are not likely to occur on a hard-bedded ice sheet. There is no dependency on ice thickness.

Interpretation of scenario 1

This end-member scenario shows that sliding ice cannot realistically disintegrate rock hills without subhorizontal fractures. In nature such rock hills will be eroded by abrasion alone, and form smooth whalebacks as opposed to roches moutonnées. The height of such hills is constrained by the vertical fracture spacing of the bedrock, which is normally <5–10 m (Jern, 2004; Krabbendam and others, 2021), so this scenario is likely only applicable to low (<5 m) hills.

Scenario 2: hemisphere with continuous, transmissive basal fracture

In hemispherical obstacles with continuous basal fractures (Fig. 3b), the resisting forces are controlled by the Coulomb rock–rock friction along the basal fracture (Eqns (12) and (15b)). They decrease linearly with relative water pressure P_w/P_i, and become zero just beyond the point of flotation ($P_w = P_i$), because of the buoyant weight F_{bz} of the obstacle (Figs 6a, b; shown for ice thickness of 300 and 600 m). Drag force F_d increases linearly as a function of sliding speed U (Eqn (3)), as in scenario 1 (Fig. 5). Lines of equal drag and resisting force as a function of sliding velocity and relative water pressure for this scenario are given by combining Eqns (3) and (15b):

$$3\pi\eta U r = \mu_{rr} \left[\frac{2}{3} \pi\, r^3\, (\rho_r - \rho_w)g + g h_i \rho_i \left(1 - \frac{P_w}{P_i}\right) \pi\, r^2 \right] \tag{20}$$

As function of sliding speed, F_d equals F_r if:

$$U = \mu_{rr} \frac{[(2/3)\, r^2\, (\rho_r - \rho_w)g + g h_i \rho_i (1 - P_w/P_i)\, r\,]}{3\eta} \tag{21}$$

Interpretation of scenario 2

The plots (Figs 6c, d) show that under a wide range of realistic conditions (boxes in graph), blunt, hemispherical obstacles with a continuous basal fracture can be removed by sliding ice. Small obstacles are considerably easier to move than large obstacles. Block removal can occur without overpressure: a small obstacle ($r = 3$) can be removed at sliding speeds of 200 m a^{-1}, with $P_w/P_i = 0.9$; these are fairly normal circumstances for ice sheets. Ice thickness has only a minor effect: a doubling of the ice thickness leads to slightly higher resisting forces, but at higher water pressures this has little effect, and in the further modelling we only model with ice thickness of 300 m. In the case of overpressure (e.g. $P_w/P_i = 1.05$, which has been observed below the GrIS), *all* obstacles would be removed regardless of size. Given that the base of the ablation zone of the GrIS is rough (e.g. Lindbäck and Pettersson, 2015; Cooper and others, 2019), and there is still a residual terrain roughness (relative relief) with amplitudes of 5–20 m in eastern Sweden with a multitude of surviving roches moutonnées (Hall and others, 2019), this scenario is not realistic as a general case. The critical assumption in this scenario, namely that of a perfectly *continuous* and horizontal basal fracture in which P_w equalises perfectly with P_w at the ice–bed interface, is likely not common in basement gneiss terrain, and should be seen as an idealised end-member scenario.

Scenario 3a: hemisphere with part intact rock and part basal fracture

This scenario considers a rock hill with a discontinuous basal fracture, with part of the basal foot print comprising intact rock

https://doi.org/10.1017/jog.2022.49 Published online by Cambridge University Press

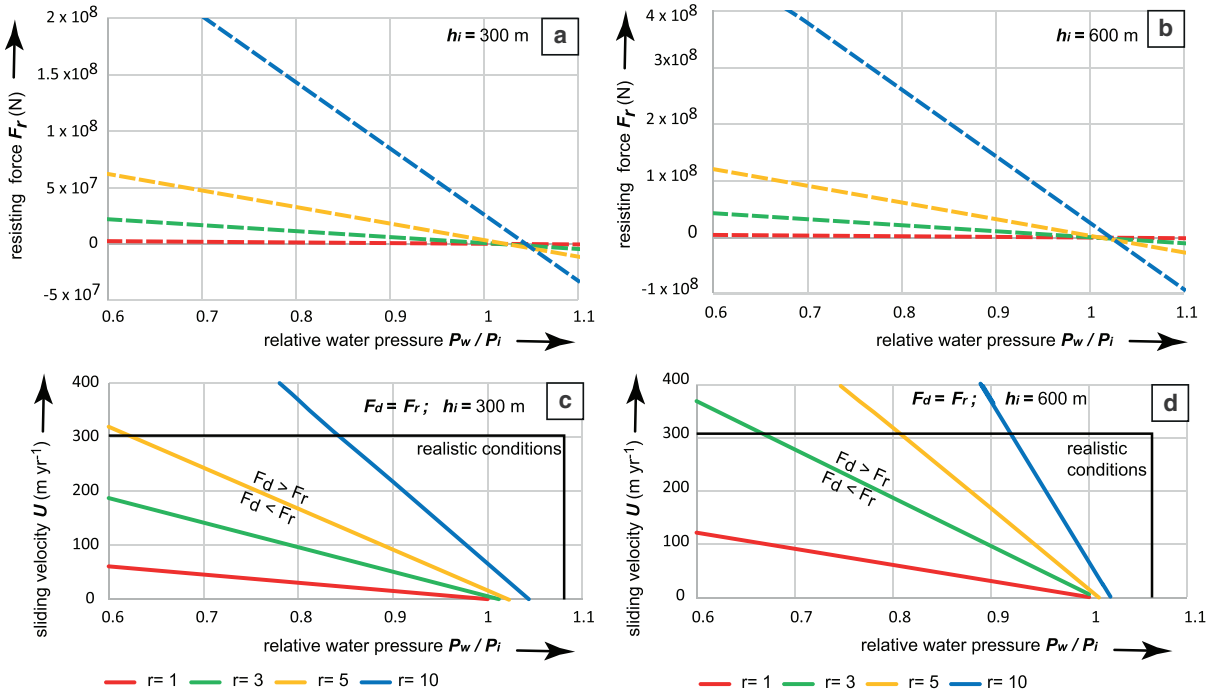

Fig. 6. (a) Resisting forces (N) as a function of relative water pressure P_w/P_i, for hemispherical obstacles with radii 1–10 m; ice thickness 300 m; Eqn (15b). (b) Same as (a), but ice thickness is 600 m. (c) Lines of equal drag and resisting forces ($F_d = F_r$) as a function of sliding speed U and relative water pressure P_w/P_i, for hemispherical obstacles with radii 1–10 m; Eqn (21). Above the lines, blocks can move, below the lines, blocks cannot move. Box indicates realistic conditions, e.g. water pressure variations between 60 and 105%, and sliding speeds <300 m a^{-1}. (d) Same as (c), for ice thickness 600 m. Figure © Svensk Kärnbränslehantering. Reproduced with permission.

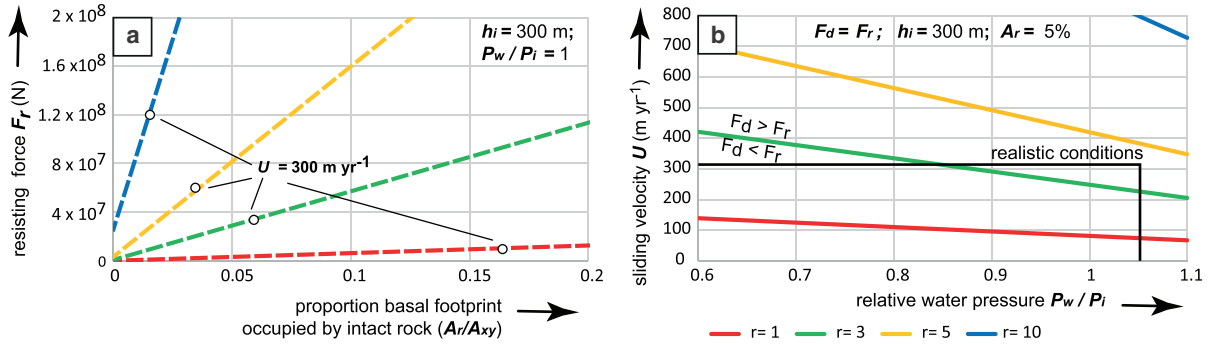

Fig. 7. (a) Resisting forces as a function of the proportion of basal footprint of hemisphere (radii 1–10 m) occupied by intact rock A_r/A_{xy}, for $P_w = P_i$ (flotation); Eqn (19b). Points are the maximum drag forces for sliding speeds of 300 m a^{-1}. (b) Lines of equal drag and resisting forces ($F_d = F_r$) as a function of sliding speed U and relative water pressure P_w/P_i, for hemispherical obstacles with radii 1–10 m with 5% of footprint occupied by intact rock; Eqn (22). Above the lines, blocks can move. Box indicates realistic conditions. Figure © Svensk Kärnbränslehantering. Reproduced with permission.

(Fig. 3c), the strength of which is controlled by the shear strength τ_r of intact gneiss. We take a value of 20 MPa: weaker rocks will have lower values. Lines of equal drag and resisting force are then given by combining Eqns (3) and (19b):

maximum. For large hemispheres (r = 5–10 m), blocks cannot move if *c.* 10% of the footprint is occupied by intact rock, for smaller blocks this can increase up to 15–20%. On the graph showing sliding velocity versus relative water pressure for equal

$$U = \frac{r\tau_r\,(A_r/A_{xy}) + (A_j/A_{xy})\,\mu_{rr}\,[(2/3)r^2(\rho_r - \rho_w)g + gh_i\rho_i(1 - P_w/P_i)r]}{3\eta} \quad (22)$$

Interpretation of scenario 3a

The graph (Fig. 7a) plotting resisting force as a function of the proportion of intact rock versus basal fracture at the base of the hemisphere (for $P_w = P_i$, i.e. flotation) shows that even a very small proportion (A_r = 5–10%) of intact rock has a dramatic effect on the resisting forces. The points show the drag force exerted by ice sliding at 300 m a^{-1} for the different radii, taken as a

drag and resisting forces (Fig. 7b) it is clear that larger (>3 m) hemispheres in essence cannot be moved under realistic conditions (box) if intact rock occupies more than 5% of the footprint. Overall, this shows that intact rock offers far more resistance than a continuous transmissive fracture. It also implies that irregularities on basal fractures, such as a small up-ice facing step, can effectively 'lock' an obstacle in place.

https://doi.org/10.1017/jog.2022.49 Published online by Cambridge University Press

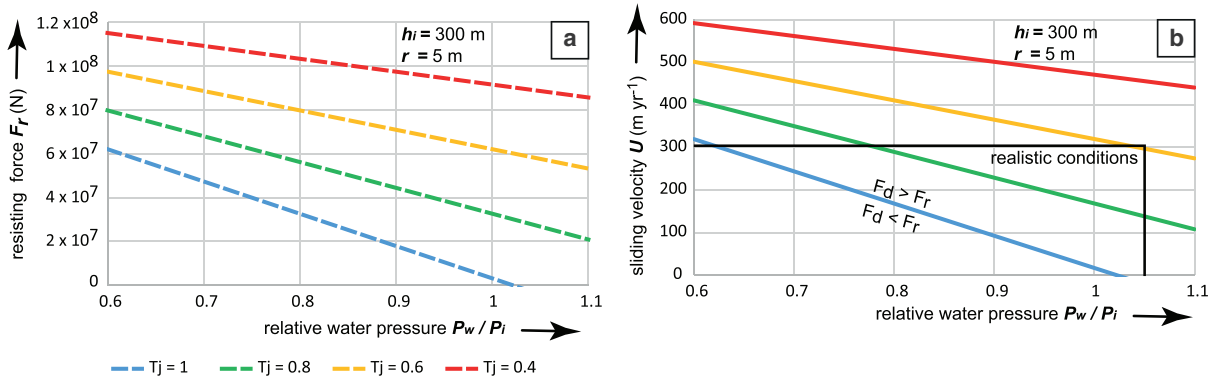

Fig. 8. Effect of limited transmissivity along basal fractures; ice thickness 300 m; hemispherical obstacle with $r = 5$. (a) Resisting force in N versus relative water pressure, with transmissivity factor T_j varying between 0.4 and 1; Eqn (16). (b) Lines where drag forces equal resisting forces ($F_d = F_r$) as a function of sliding speed U and relative water pressure P_w/P_i, for hemispherical obstacles with 5 m radius, with transmissivity factor T_j between 0.4 and 1; Eqn (21) with T_j, as per Eqn (16). Above the lines, blocks can move. Box indicates realistic conditions. Figure © Svensk Kärnbränslehantering. Reproduced with permission.

Scenario 3b: hemisphere with low-transmissivity basal fracture

The effects of limited fracture transmissivity are assessed by varying a transmissivity factor T_j; $T_j = 1$ for perfect transmissive fractures in which water pressure equalises instantaneously with water pressure fluctuations at the ice–bed contact; $T_j = 0$ for completely tight, clogged fractures, that remain unconnected to the ice bed, as per Eqn (16).

Interpretation of scenario 3b

From the graphs (Fig. 8), it is evident that fracture transmissivity is an important factor. A lower transmissivity index limits the maximum pressures within the fractures (and also hampers hydraulic jacking), so that resisting forces are not lowered during water pressure fluctuations at the ice bed. In the balance of drag and resisting forces, this implies that much higher sliding speeds would be required to mobilise roches moutonnées. With transmissivities below 0.6, mobilisation becomes unrealistic.

Scenario 4: elongate obstacle with continuous basal fracture

For an elongate, flat-topped cuboid obstacle, the drag and resisting forces are expressed in terms of length L, width W and height H of the obstacle. The drag force is a combination of viscous drag F_{vd} acting on the stoss surface area with surface $H \times W$, and Coulomb friction F_{cf} acting on the flat top surface (Fig. 3d) with surface $L \times W$, and being dependent on the relative water pressure, as per Eqn (10b). The resisting force is a function of the mass of the obstacle, with volume $H \times W \times L$, and the normal stress exerted by the ice acting on the top surface, with surface area $L \times W$, as per Eqn (15c).

The graph for an obstacle with fixed height (2 m), but variable length (Fig. 9a), shows that while the total drag force F_d depends somewhat on the length of the obstacle, this dependence is weak. This shows that most of the drag force is provided by the viscous drag acting on the stoss side (dependent on the stoss surface area), whereas Coulomb friction on the top surface (which increases with increasing area of the top surface and hence length) only makes a minor contribution to the total drag force. Figure 9b shows that the drag forces decrease slightly with increasing water pressure, as the Coulomb friction drag component is decreasing.

Lines of equal drag and resisting forces as a function of sliding velocity become (combining Eqns (10b) and (15c)):

$$U = \frac{\mu_{rr}\, HWL\,(\rho_r - \rho_w)g + \mu_{rr}\, gh_i\rho_i(1 - P_w/P_i)LW - \mu_{ir}gh_i\rho_i(1 - P_w/P_i)LW}{3\eta\sqrt{2HW/\pi}} \tag{23}$$

For simplicity, we test an elongate rock hill with $W = 5$ m and $H = 2$ m, but with variable length, noticing that the width plays little role. However, drag forces are little affected by the obstacle length; the resisting forces are strongly dependent on it: as a consequence longer obstacles are more difficult to move than shorter ones (Fig. 9c). Nevertheless, as water pressure in the fractures increases, increasingly long obstacles can be moved (Figs 9d, e): at flotation ($P_w = P_i$) within the fractures, long obstacles can be removed at sliding velocities of 50–100 m a^{-1}.

Interpretation of scenario 4

Long obstacles are more difficult to remove than short obstacles: removal requires high sliding velocities and high water pressures in basal fractures: at flotation ($P_w = P_i$), elongate obstacles up to 100 m can be removed at sliding velocities of 200 m a^{-1}, provided that basal fractures are transmissive and continuous.

Scenario 5: rock steps on a flat surface

In this scenario we look at the flat-topped surface, which may be part of a larger rock hill, or a low-relief rock surface. Overpressure and hydraulic jacking can partially uplift a single block (Leijon, 2005; Forssberg and others, 2007), so that a small rock step, with an up-ice facing stoss side, protrudes above the previously flat surface (Fig. 2e). The drag force on that flat-topped surface, that previously only comprised of Coulomb friction, now has an added component of viscous drag acting on the up-ice facing rock step (Fig. 3e). The question is whether this added viscous drag force is sufficiently high to be able to disintegrate the top surface of the rock.

The drag force exerted on the top surface, with a rock step with height H_s is given by:

$$F_d = 3\,\eta U\sqrt{2H_s W/\pi} + \mu_{ir}gh_i\rho_i\left(1 - \frac{P_w}{P_i}\right)WL_n \tag{24}$$

where L_n is the total length of the row of blocks down-ice of the uplifted block (Fig. 3e). Since the rock mass is already opened up

https://doi.org/10.1017/jog.2022.49 Published online by Cambridge University Press

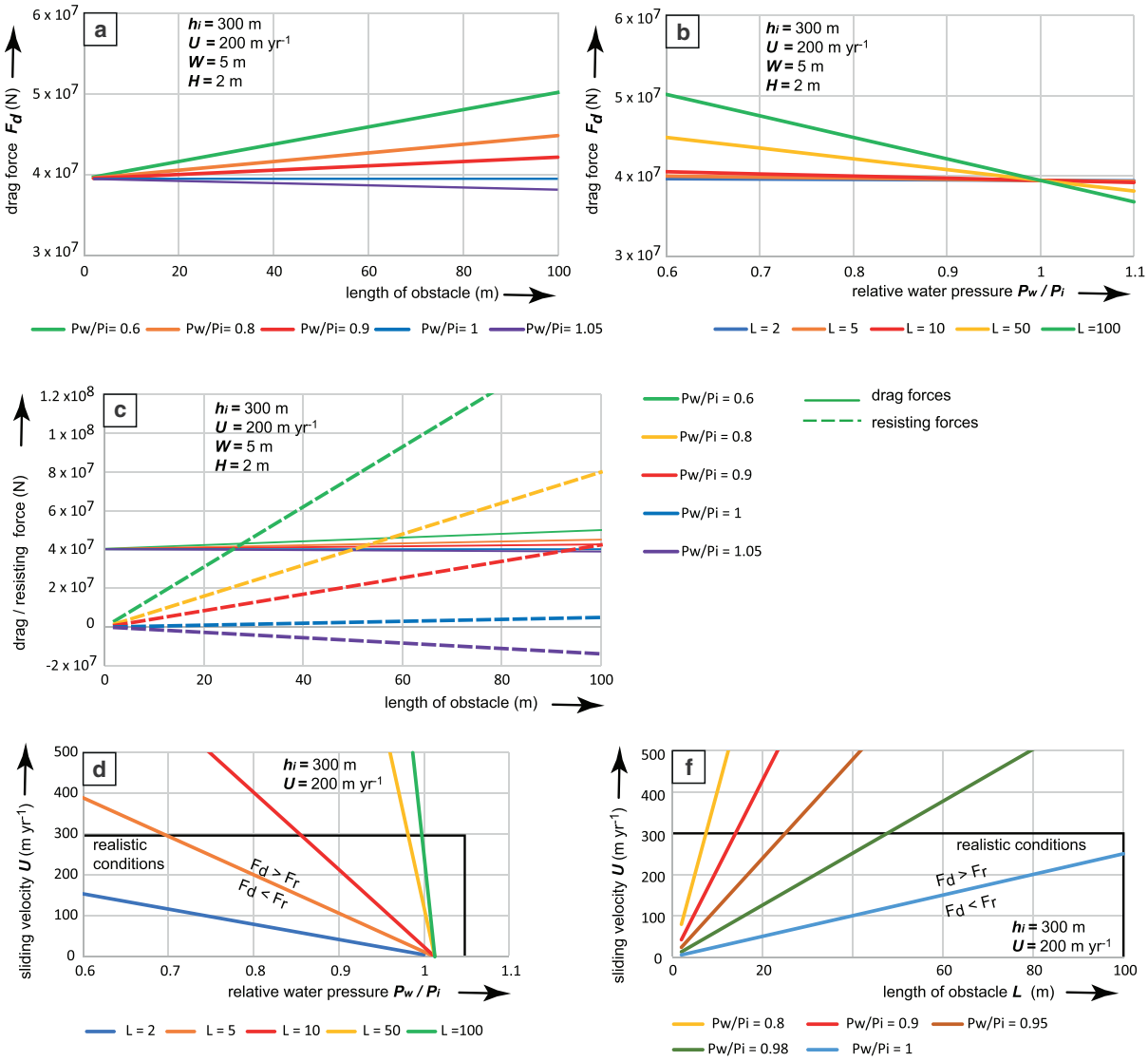

Fig. 9. (a) Drag forces (N) as a function of length of an elongate obstacle, for different relative water pressures; $W = 5$, $H = 2$ m, $h_i = 300$ m, sliding velocity $U = 200$ m a^{-1}; Eqn (10b). (b) Drag forces as a function of relative water pressure, for obstacles with different lengths; other conditions same as (a); Eqn (10b). (c) Resisting forces (dashed lines; Eqn (15c)) and drag forces (solid lines; Eqn (10b)) as a function of length of a rectangular obstacle ($W = 5$, $H = 2$ m), for different relative water pressures P_w/P_i; ice thickness 300 m; ice sliding velocity 200 m a^{-1}. (d) Lines of equal drag and resisting forces ($F_d = F_r$) as a function of sliding speed U and relative water pressure P_w/P_i, for rectangular obstacles; Eqn (23). Above the lines, blocks can move. Box indicates realistic conditions. (e) Lines of equal drag and resisting forces ($F_d = F_r$) as a function of sliding speed U and obstacle length, for different relative water pressures P_w/P_i (0.8–1.05); Eqn (23). Figure © Svensk Kärnbränslehantering. Reproduced with permission.

to allow hydraulic jacking we assume a transmissivity of 1. The resisting forces of the row of blocks down-ice from the uplifted blocks is given by:

$$F_{rj} = \mu_{rr}\left[HWL_n\,(\rho_r - \rho_w)g + gh_i\rho_i\left(1 - \frac{P_w}{P_i}\right)WL_n\right] \quad (25)$$

Lines of equal drag and resisting forces as a function of sliding velocity become (Eqns (1), (24) and (25)):

$$U = \frac{\mu_{rr}\,HWL_n\,(\rho_r - \rho_w)g + (\mu_{rr} - \mu_{ir})\,g\,h_i\rho_i(1 - P_w/P_i)WL_n}{3\eta\sqrt{2HsW/\pi}} \quad (26)$$

Interpretation of scenario 5

The drag forces exerted on a flat surface rise rapidly when a small (*c.* 0.1 m high) rock step is created (Fig. 10a), due to the increase in viscous drag. This relationship is proportional to the inverse of the square root of the height of the rock step. Clearly, the drag forces exerted on a small step are significant. Interestingly, drag forces drop slightly with higher water pressures (Fig. 10b), because Coulomb friction on the top surface decreases with increasing water pressure. The lines of balanced drag and resisting forces (Fig. 10c) show that a series of blocks with cumulative length of blocks of <10 m can be removed with sliding velocities <200 m a^{-1} when a 0.1–0.4 m high rock step is introduced. Under overpressure ($P_w/P_i = 1.02$ as shown in Fig. 10d), such block removal can occur at sliding velocities <100 m a^{-1}. The introduction of a rock step by hydraulic jacking thus radically increases the drag forces exerted on smooth, flat rock surfaces, and may thus assist in glaciotectonic disintegration of larger rock hills.

Discussion

Favourable conditions for glacial ripping

We modelled the drag and resisting forces acting on rock hills of various sizes and shapes, and how variable water pressures in fractures affect resisting forces and lead to glaciotectonic failure of the

https://doi.org/10.1017/jog.2022.49 Published online by Cambridge University Press

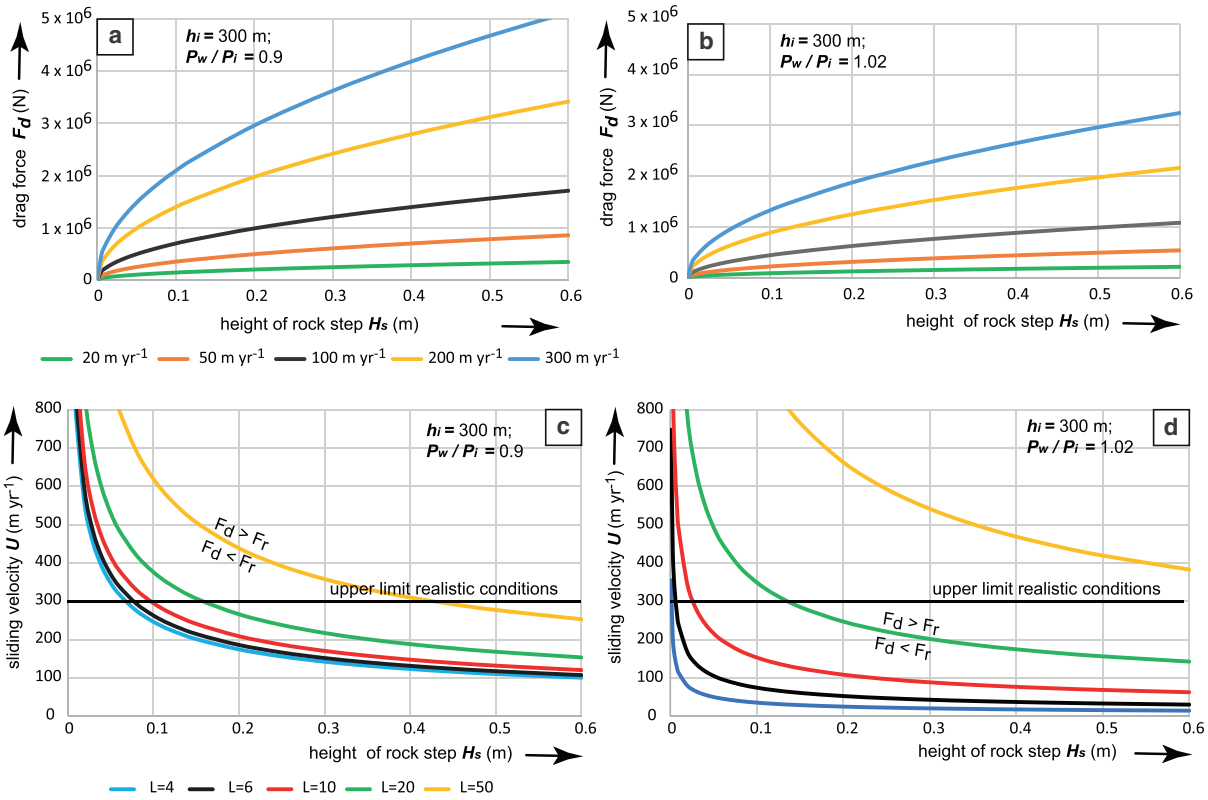

Fig. 10. (a) Drag forces (N) on a flat surface with a rock step, as a function of height of rock step H_s, for different ice velocities; Eqn (24). Width and height of blocks are 5 and 2 m; ice thickness = 300 m, $P_w/P_i = 0.9$. (b) Same as (a), with $P_w/P_i = 1.02$ (2% overpressure). (c) Lines of equal drag and resisting forces ($F_d = F_r$) as a function of sliding velocity and height of rock step, for different cumulative length of blocks, $P_w/P_i = 0.9$; Eqn (26). (d) Same as (c), with $P_w/P_i = 1.02$ (2% overpressure). Figure © Svensk Kärnbränslehantering. Reproduced with permission.

rock mass. Ice drag forces increase with ice sliding velocity, so fast-flowing ice can remove larger or more resistant rock hills than slow-moving ice. Ice drag forces also increase with the radius of a hemispherical obstacle (or the stoss-side surface area), so that high rock hills are more vulnerable to removal than low, streamlined ones. This is consistent with (1) observations that hard beds of palaeo-ice streams are typically streamlined along the palaeo-ice flow lines (Bradwell, 2013; Krabbendam and others, 2016); and (2) the absence of high, blunt roches moutonnées with clear continuous basal fractures in eastern Sweden.

Resisting forces are a function of the shape and size of the hill, the fracture pattern of the rock hill (in particular the presence of continuous subhorizontal fractures) and the (peak) water pressure within the fractures. Our modelling indicates that a rock hill without a continuous subhorizontal fracture cannot be moved under plausible subglacial conditions. Such a rock hill is likely to be eroded by abrasion alone, forming whalebacks.

In contrast, a rock hill with a continuous, smooth subhorizontal fracture is easily removed by sliding ice at relatively low sliding velocities, even without overpressured water. However, long, smooth fractures are probably rare in nature, in particular in basement gneisses: rock bridges, up-ice facing steps in the subhorizontal fractures, or indeed very rough fracture surfaces (cf. Barton and Choubey, 1977) all increase the resisting forces, hindering rock removal. Thus, such a scenario is likely only applicable to small, blunt rock hills: an example is the glacial modification of granite tors by removal of superstructure to leave low-profile plinths (Hall and Phillips, 2006).

Our modelling shows that elongate rock hills have a higher resisting force, due to the larger rock mass resting on the basal fracture, and greater likelihood of mentioned irregularities along basal fractures. Increased water pressures within a continuous basal fracture greatly reduce resisting forces of a rock hill. Disintegration of larger and/or elongate rock hills, or with more rough basal fractures is thus possible, in particular if pressure fluctuations result in hydraulic jacking. Hydraulic jacking will thus act as a trigger for glaciotectonic deformation. Favourable glaciological conditions for hydraulic jacking include high duration, volume and amplitude of overpressure events at the ice bed. Partial disintegration of a larger rock hill may also occur if hydraulic jacking uplifts a single block, creating a small rock step protruding above the flat top surface. Such a small step dramatically increases the drag forces exerted on the top surface and can aid (partial) disintegration of that rock hill, even if the hill as a whole is too resistant to be moved.

Glacial ripping is thus plausible under certain favourable conditions: a combination of fast ice sliding velocities (>50 m a^{-1}), high water pressures within fractures and favourable fracture patterns in the rock hill, in particular continuous subhorizontal fractures. The glaciological conditions necessary for glacial ripping are not unusual for the base of an ice sheet. In general, sliding velocities of an ice sheet increase towards the margin (Joughin and others, 2010; Patton and others, 2017), as do the frequency and magnitude of overpressure events (e.g. Claesson Liljedhal and others, 2016), so that glacial ripping is more likely near the margin and at the end of a glaciation, consistent with field evidence in Sweden. However, given a certain maximum relative overpressure (say 110%; Wright and others, 2016), the maximum depth of overpressure within the rock is limited to ~3% of ice thickness, which diminishes the effectiveness of hydraulic jacking at low ice thickness.

Favourable geological conditions include the presence of transmissive and continuous basal fractures. Long transmissive subhorizontal fractures do occur in basement rock, but only locally so (Carlsson, 1979; Follin and others, 2007; Goodfellow and others, 2019; Krabbendam and others, 2021). Such conditions, however, are common for flat lying sedimentary rocks, where subhorizontal

https://doi.org/10.1017/jog.2022.49 Published online by Cambridge University Press

bedding planes take the role of the basal fractures. Glacial ripping events have been documented in such rocks in NW Scotland and Ontario respectively (Bukhari and others, 2021; Hall and others, 2021).

The glaciological conditions favourable for glacial ripping (thawed base, fast sliding velocity, high water pressures), are likely to cause lee side cavitation so similar conditions are also favourable for plucking. Cavitation makes little difference to the drag forces, as these are generated at the stoss side of the rock hill or rock steps. However, cavities represent reservoirs with water available to enter fractures, so the presence of cavities should facilitate hydraulic jacking. The presence of cavities may also have other, more complex but secondary, effects on the force balance discussed here. Some, but not all, observed disintegrated roches moutonnées in eastern Sweden show increased disintegration towards the presumed cavities (Krabbendam and others, 2022), which can be partially explained by water entry from lee side cavities.

Effects of non-modelled parameter variability

For some parameters, variability has not been modelled explicitly, but their effects can be discussed qualitatively given the relative simplicity of the equations.

Although we model ice as a Newtonian medium with a fixed viscosity appropriate for temperate ice, it is possible that cold ice overlies a sliding ice base, separated by a thin layer (<1 m) of temperate ice. In that case, the effective viscosity of ice creeping around the obstacles is much higher, possibly by a factor of 10 or more (Glen, 1955; Morgan, 1991; Krabbendam, 2016). In such a situation, the drag forces on the rock obstacle would be much higher. While ice sliding velocities may be lower in such a scenario, we note that a sliding velocity of 10 m a^{-1} with a high-viscosity 'cold-ice rheology' would exert drag forces of similar magnitude as a sliding velocity of 100 m a^{-1} with a 'temperate-ice rheology', as per Eqn (3).

Ice–rock friction coefficient was taken at 0.05, but higher values (up to 0.4) have been measured in experiments with large debris particle size and high particle concentrations (Emerson and Rempel, 2007). A higher ice–rock friction coefficient would result in higher drag forces exerted on the rock obstacles and thus potentially aid glacial ripping, although this effect diminishes at high water pressures at the ice bed (Eqns (10a) and (10b)).

Rock–rock friction coefficient along the fractures was taken at 0.7, which is average for basement rocks. Many other rock types show a rock–rock lower friction coefficient (0.4–0.6; Ramana and Gogte, 1989), which would evidently facilitate glacial ripping. The converse is also the case: a higher fracture roughness would increase the friction coefficient, while very high fracture coefficients are transient to a situation with part intact rock (e.g. scenario 3a), or a rock bridge. Fracture roughness and rock–rock friction thus potentially play an important role in controlling glacial ripping, but are poorly constrained in the field, and difficult to predict.

Intact rock strength was taken as the average for basement gneisses. Gneisses, however, are among the strongest rocks occurring in bulk at the Earth surface: most other rock types will have a lower intact rock strength, thus potentially facilitating glacial ripping. A number of papers have recorded a form of glaciotectonic disintegration affecting the top few metres of weaker bedrock such as mudstone or sandstone (e.g. Croot and Sims, 1996; Hiemstra and others, 2007). On the other hand, the effect of the intact rock strength in the case of a stepped fracture geometry is so pronounced (see scenario 3a), that such as step will still hamper glacial ripping except for the weakest rocks (e.g. shales, chalk). Such rocks, however, are also vulnerable to abrasion and plucking to such a degree that a distinction between erosion mechanisms may become less meaningful (Krabbendam and Glasser, 2011).

Fracture transmissivity and in-plane rock bridges

In most modelled scenarios, glacial ripping requires high water pressure to penetrate the fractures in the shallow rock mass: such penetration depends on the duration, number and amplitude of high-pressure events at the bed, but also on the fracture transmissivity. Low-transmissivity fractures attenuate water pressure transients at the ice–bed, and water pressure within the fracture may not equalise rapidly enough to result in overpressure *within* the fracture, even if overpressure conditions occur temporarily at the ice bed. Field evidence in eastern Sweden shows that, at least locally, fractures were sufficiently transmissive to allow hydraulic jacking (Carlsson, 1979, Follin and others, 2007; Forssberg and others, 2007; Krabbendam and others, 2021). However, the responses of fractures to water pressure transients at the ice bed are potentially complex and not known from subglacial measurements. Fracture transmissivity may be low because fractures are tight, are sealed with fracture fills, or have rock bridges. Studies in hydro-tunnels in Norway, with comparable overall water pressure fluctuations, provide an instructive analogue. Neupane and others (2020) compared water pressures in a hydro-tunnel with those in boreholes 2–4 m in the tunnel wall. Responses to pressure fluctuations in the tunnel were bimodal: some boreholes showed a delayed or virtually no response, whereas other boreholes showed a very rapid response to pressure transients in the tunnel. Thus, some boreholes intersected non-transmissive fractures, whereas others intersected highly transmissive fracture(s). The bimodality of the responses likely relates to the 'cubic law', which states that fracture transmissivity is proportional to the cube of fracture aperture, and hence strongly non-linear (Witherspoon and others, 1980). From the tunnel experiments of Neupane and others (2020) it is not known if fractures can progressively increase their transmissivity under repeated pressure transients, but a long-term increase in rock falls in hydro-tunnels subjected to pressure transients (Bråtveit and others, 2016) suggests this is plausible. Translated to the subglacial setting discussed here, these studies imply that (1) overpressure in rock fractures by external pressure transients is possible, (2) the transmissivity of fractures is broadly bimodal ('open' or 'shut') and (3) it may be possible that fractures can be opened progressively due to repeated pressure transients.

Effects of till over

The preceding discussion deals with bare rock surfaces but till cover occurs, if patchily, across basement rocks of eastern Sweden (e.g. Sohlenius and others, 2004; Kleman and others, 2008). Till-overlying bedrock would have two effects. Firstly, the effect of overpressure at the ice bed will be attenuated, and may not reach the bedrock, in particular if the till is consolidated. However, if till occurs only in the lee side of an obstacle, water may still enter the rock hill through fractures on the lateral sides. Secondly, a layer of actively deforming till (which may overlie a layer of consolidated, non-deforming till – see Evans and others, 2006), will take up much of the drag forces exerted by the ice, and reduce the drag forces exerted on the bedrock. This latter point is consistent with the survival of dilated fractures and brecciated rock below till at several sites in eastern Sweden (Carlsson, 1979; Krabbendam and others, 2021). Generally, extensive till cover would hamper glacial ripping.

https://doi.org/10.1017/jog.2022.49 Published online by Cambridge University Press

Erosion by early glaciation versus repeated glaciations: the fate of vulnerable rock hills

Most deglaciated terrains have been repeatedly glaciated and subjected to several phases of subglacial erosion. What would have happened during the early glaciations? In Europe and North America, vulnerable, high, blunt rock hills such as tors are common outside Pleistocene glacial limits, or occur in areas previously occupied by cold ice, characterised by minimal long-term ice-sheet erosion (Hättestrand and Stroeven, 2002; Briner and others, 2003; Hall and Phillips, 2006; Darmody and others, 2008). However, they are absent in areas that have been (repeatedly) covered by warm-based Pleistocene ice sheets, suggesting they were removed by glacial erosion during early Pleistocene ice-sheet cover, together with vulnerable layers of regolith (e.g. Clark and Pollard, 1998).

The modelling shows that vulnerable, high, blunt rock hills are easily removed by glacial ripping: scenario 2 shows this is possible even without overpressure and hydraulic jacking, provided the rock hill possessed continuous subhorizontal fractures. However, once such vulnerable rock hills are removed, it is likely that other, more resistant rock hills cannot be removed without high water pressures and hydraulic jacking. The blunt rock hills that presently remain all have more complicated, 'stepped' fracture patterns (Krabbendam and others, 2022). In other words, glacial ripping operating in areas subjected to previous phases of subglacial erosion requires the three-stage process including overpressure as set out by Hall and others (2020) to be effective.

To constrain or model the response of a rock mass to subglacial erosion, its fracture patterns and their variability must be understood (e.g. Dühnforth and others, 2010; Hooyer and others, 2012; Iverson, 2012) but generalised assumptions on fracture density may be unrealistic. To robustly constrain the vulnerability of a rock mass to subglacial erosion in specific locations, such as planned nuclear waste repositories, quantitative measurements on fracture patterns are recommended.

Conclusions

Modelling of ice drag forces and resisting forces of rock obstacles of different size and fracture patterns shows that it is physically plausible for sliding ice at the base of an ice sheet to remove or disintegrate rock hills, resulting in glacial ripping. Glaciological factors that favour rock hill removal are: (1) fast flowing ice; (2) high water pressure, in particular overpressure events; these conditions are commonly met below the ablation zone of ice sheets. Ice drag forces increase with stoss-side surface area of an obstacle so that high, blunt rock hills are more vulnerable to glacial ripping than low, streamlined ones. However, the resisting forces of a hill play a critical role and are dependent on the fracture patterns of the bedrock. Geological factors that lower the resisting forces and thus favour rock hill disintegration are: (1) presence of continuous subhorizontal fractures; (2) high fracture transmissivity, so that water pressure fluctuations at the ice bed can penetrate into the rock mass, and aid hydraulic jacking and disintegration. Glacial ripping is a physically plausible mechanism that can be seen as a form of glaciotectonics, but also as an erosion mechanism in itself, controlled by different factors than abrasion and plucking.

Acknowledgements. Andrew Finlayson is thanked for comments on an earlier version of the manuscript. We thank two anonymous reviewers and the editor for thorough and constructive reviews. MK, FD, CA and SR publish with permission of the Executive Director of BGS.

This work was supported by the Svensk Kärnbränslehantering AB, as part of a SKB-funded project on glacial ripping.

References

Alley RB, Cuffey KM and Zoet LK (2019) Glacial erosion: status and outlook. *Annals of Glaciology* **60**(80), 1–13. doi: 10.1017/aog.2019.38

Andrén T and 5 others (2011) The development of the Baltic Sea Basin during the last 130 ka. In Harff J, Björck S and Hoth P (eds), *The Baltic Sea Basin*. Berlin: Springer, pp. 75–97.

Andrews LC and 7 others (2014) Direct observations of evolving subglacial drainage beneath the Greenland ice sheet. *Nature* **514**(7520), 80–83. doi: 10.1038/nature13796

Bagheri G and Bonadonna C (2016) On the drag of freely falling non-spherical particles. *Powder Technology* **301**, 526–544. doi: 10.1016/j.powtec.2016.06.015

Barton N and Choubey V (1977) The shear strength of rock joints in theory and practice. *Rock Mechanics* **10**(1), 1–54.

Bradwell T (2013) Identifying palaeo-ice-stream tributaries on hard beds: mapping glacial bedforms and erosion zones in NW Scotland. *Geomorphology* **201**, 397–414. doi: 10.1016/j.geomorph.2013.07.014

Bråtveit K, Bruland A and Brevik O (2016) Rock falls in selected Norwegian hydropower tunnels subjected to hydropeaking. *Tunnelling and Underground Space Technology* **52**, 202–207. doi: 10.1016/j.tust.2015.10.003

Brideau M-A, Yan M and Stead D (2009) The role of tectonic damage and brittle rock fracture in the development of large rock slope failures. *Geomorphology* **103**(1), 30–49. doi: 10.1016/j.geomorph.2008.04.010

Briner J, Miller G, Davis PT, Bierman P and Caffee M (2003) Last Glacial Maximum ice sheet dynamics in Arctic Canada inferred from young erratics perched on ancient tors. *Quaternary Science Reviews* **22**(5–7), 437–444. doi: 10.1016/S0277-3791(03)00003-9

Bukhari S and 6 others (2021) Regional subglacial quarrying and abrasion below a paleo ice stream crossing the shield-Paleozoic boundary of central Canada: the importance of substrate control. *Boreas* **50**(3), 781–805. doi: 10.1111/bor.12522

Byers J, Cohen D and Iverson NR (2012) Subglacial clast/bed contact forces. *Journal of Glaciology* **58**(207), 89–98. doi: 10.3189/2012JoG11J126

Carlsson A (1979) Characteristic features of a superficial rock mass in southern Sweden. *Striae* **11**, 1–79 .

Chandler D, Hubbard B, Hubbard A, Murray T and Rippin D (2008) Optimising ice flow law parameters using borehole deformation measurements and numerical modelling. *Geophysical Research Letters* **35**, L12502. doi: 10.1029/2008GL033801.

Claesson Liljedahl L and 9 others (2016) The Greenland Analogue Project: final report. SKB Report TR-14-13, Svensk Kärnbränslehantering AB.

Clark PU and Pollard D (1998) Origin of the middle Pleistocene transition by ice sheet erosion of regolith. *Paleoceanography and Paleoclimatology* **13**(1), 1–9. doi: 10.1029/97PA02660

Cohen D and 5 others (2005) Debris-bed friction of hard-bedded glaciers. *Journal of Geophysical Research: Earth Surface* **110**, F02007. doi: 10.1029/2004JF000228

Colbeck SC and Evans RJ (1973) A flow law for temperate glacier ice. *Journal of Glaciology* **12**(64), 71–86. doi: 10.3189/S0022143000022711

Cooper MA and 5 others (2019) Subglacial roughness of the Greenland ice sheet: relationship with contemporary ice velocity and geology. *The Cryosphere* **13**(11), 3093–3115. doi: 10.5194/tc-13-3093-2019

Croot DG and Sims P (1996) Early stages of till genesis: an example from Fanore, County Clare, Ireland. *Boreas* **25**(1), 37–46. doi: 10.1111/j.1502-3885.1996.tb00833.x

Cuffey K and Patterson W (2010) *The Physics of Glaciers*. Burlington, MA: Elsevier.

Darmody RG and 5 others (2008) Age and weathering status of granite tors in Arctic Finland (~68°N). *Geomorphology* **94**(1-2), 10–23. doi: 10.1016/j.geomorph.2007.04.006

Das SB and 6 others (2008) Fracture propagation to the base of the Greenland ice sheet during supraglacial lake drainage. *Science* **320**(5877), 778–781. doi: 10.1126/science.1153360

Dewandel B, Lachassagne P, Wyns R, Maréchal J-C and Krishnamurthy NS (2006) A generalized 3-D geological and hydrogeological conceptual model of granite aquifers controlled by single or multiphase weathering. *Journal of Hydrology* **330**(1-2), 260–284. doi: 10.1016/j.jhydrol.2006.03.026

Dioguardi F, Mele D and Dellino P (2018) A new one-equation model of fluid drag for irregularly shaped particles valid over a wide range of

Reynolds number. *Journal of Geophysical Research: Solid Earth* **123**(1), 144–156. doi: 10.1002/2017JB014926

Doyle SH and 9 others (2013) Ice tectonic deformation during the rapid in situ drainage of a supraglacial lake on the Greenland ice sheet. *The Cryosphere* **7**(1), 129–140. doi: 10.5194/tc-7-129-2013

Dühnforth M, Anderson RS, Ward D and Stock GM (2010) Bedrock fracture control of glacial erosion processes and rates. *Geology* **38**, 423–426. doi: 10.1130/G30576.1

Elmo D, Donati D and Stead D (2018) Challenges in the characterisation of intact rock bridges in rock slopes. *Engineering Geology* **245**, 81–96. doi: 10.1016/j.enggeo.2018.06.014

Emerson LF and Rempel AW (2007) Thresholds in the sliding resistance of simulated basal ice. *The Cryosphere* **1**(1), 11–19. doi: 10.5194/tc-1-11-2007

Evans DJA, Phillips ER, Hiemstra JF and Auton CA (2006) Subglacial till: formation, sedimentary characteristics and classification. *Earth-Science Reviews* **78**(1-2), 115–176. doi: 10.1016/j.earscirev.2006.04.001

Follin S and 6 others (2007) Hydrogeological characterisation and modelling of deformation zones and fracture domains, Forsmark modelling stage 2.2. SKB Report R-07-48, Svensk Kärnbränslehantering AB.

Forssberg O and 8 others (2007) Forsmark Site Investigation: Detailed Fracture and Bedrock Mapping, Quaternary Investigations and GPR Measurements at Excavated Outcrop AFM001264. SKB Report P-05-269, Svensk Kärnbränslehantering AB.

Ganser GH (1993) A rational approach to drag prediction of spherical and nonspherical particles. *Powder Technology* **77**(2), 143–152. doi: 10.1016/0032-5910(93)80051-B

Glamheden R and 5 others (2007).Rock mechanics Forsmark. Site descriptive modelling Forsmark stage 2.2. SKB Report TR-07-31, Svensk Kärnbränslehantering AB.

Glasser NF and Bennett MR (2004) Glacial erosional landforms: origins and significance for palaeoglaciology. *Progress in Physical Geography* **28**(1), 43–75. doi: 10.1191/0309133304pp401ra

Glen JW (1955) The creep of polycrystalline ice. *Proceedings of the Royal Society of London, Series A. Mathematical and Physical Sciences* **228** (1175), 519–538. doi: 10.1098/rspa.1955.0066

Goodfellow BW and 5 others (2019) Exploring alternative models for the formation of conspicuously flat basement surfaces in southern Sweden. SKB Report TR-19-22, Svensk Kärnbränslehantering AB.

Hall AM and 7 others (2019) Past and future impact of glacial erosion in Forsmark and Uppland. SKB Report TR-19-07, Svensk Kärnbränslehantering AB.

Hall AM and 8 others (2020) Glacial ripping: geomorphological evidence from Sweden for a new process of glacial erosion. *Geografiska Annaler: Series A, Physical Geography* **102**(4), 333–353. doi: 10.1080/04353676.2020.1774244

Hall AM, Mathers H and Krabbendam M (2021) Glacial ripping in sedimentary rocks: Loch Eriboll, NW Scotland. *Geosciences* **11**(6), 232. doi: 10.3390/geosciences11060232

Hall AM and Phillips WM (2006) Glacial modification of granite tors in the Cairngorms, Scotland. *Journal of Quaternary Science* **21**(8), 811–830. doi: 10.1002/jqs.1003

Hallet B (1979) A theoretical model of glacial abrasion. *Journal of Glaciology* **23**(89), 39–50. doi: 10.3189/S0022143000029725

Harper JT, Meierbachtol T and Humphrey NF (2019) Greenland ICE Project, Final Report. SKB Report R-18-06, Svensk Kärnbränslehantering AB.

Harrington JA, Humphrey NF and Harper JT (2015) Temperature distribution and thermal anomalies along a flowline of the Greenland ice sheet. *Annals of Glaciology* **56**(70), 98–104. doi: 10.3189/2015AoG70A945

Hättestrand C and Stroeven AP (2002) A relict landscape in the centre of Fennoscandian glaciation: geomorphological evidence of minimal Quaternary glacial erosion. *Geomorphology* **44**(1-2), 127–143. doi: 10.1016/S0169-555X(01)00149-0

Hedenström A and Risberg J (2003) Shore displacement in northern Uppland during the last 6500 calendar years. SKB Report TR-03-17, Svensk Kärnbränslehantering AB.

Hiemstra JF, Evans DJ and Cofaigh CÓ (2007) The role of glacitectonic rafting and comminution in the production of subglacial tills: examples from southwest Ireland and Antarctica. *Boreas* **36**(4), 386–399. doi: 10.1080/03009480701213521

Hökmark H and Lönnqvist M (2014) Reply to comment by Christopher Talbot on 'Approach to estimating the maximum depth for glacially induced hydraulic jacking in fractured crystalline rock at Forsmark, Sweden'. *Journal of Geophysical Research: Earth Surface* **119**, 955–959. doi: 10.1002/2013JF003052

Hooyer TS, Cohen D and Iverson NR (2012) Control of glacial quarrying by bedrock joints. *Geomorphology* **153-154**, 91–101. doi: 10.1016/j.geomorph.2012.02.012

Iverson NR (2012) A theory of glacial quarrying for landscape evolution models. *Geology* **40**, 679–682. doi: 10.1130/G33079.1

Jern M (2004) Determination of the in situ block size distribution in fractured rock, an approach for comparing in-situ rock with rock sieve analysis. *Rock Mechanics and Rock Engineering* **37**(5), 391–401. doi: 10.1007/s00603-004-0029-0

Johnson MD, Ståhl Y, Larsson O and Seger S (2010) New exposures of Baltic ice lake drainage sediments, Götene, Sweden. *GFF* **132**(1), 1–12. doi: 10.1080/11035891003597067

Joughin I, Smith BE, Howat IM, Scambos T and Moon T (2010) Greenland flow variability from ice-sheet-wide velocity mapping. *Journal of Glaciology* **56**(197), 415–430. doi: 10.3189/002214310792447734

Kemeny J (2003) The time-dependent reduction of sliding cohesion due to rock bridges along discontinuities: a fracture mechanics approach. *Rock Mechanics and Rock Engineering* **36**(1), 27–38. doi: 10.1007/s00603-002-0032-2

Kleman J, Stroeven AP and Lundqvist J (2008) Patterns of Quaternary ice sheet erosion and deposition in Fennoscandia and a theoretical framework for explanation. *Geomorphology* **97**(1-2), 73–90. doi: 10.1016/j.geomorph.2007.02.049

Krabbendam M (2016) Sliding of temperate basal ice on a rough, hard bed: creep mechanisms, pressure melting, and implications for ice streaming. *The Cryosphere* **10**(5), 1915–1932. doi: 10.5194/tc-10-1915-2016

Krabbendam M and Bradwell T (2014) Quaternary evolution of glaciated gneiss terrains: pre-glacial weathering vs. glacial erosion. *Quaternary Science Reviews* **95**, 20–42. doi: 10.1016/j.quascirev.2014.03.013

Krabbendam M, Eyles N, Putkinen N, Bradwell T and Arbelaez-Moreno L (2016) Streamlined hard beds formed by palaeo-ice streams: a review. *Sedimentary Geology* **338**, 24–50. doi: 10.1016/j.sedgeo.2015.12.007

Krabbendam M and Glasser N (2011) Glacial erosion and bedrock properties in NW Scotland: abrasion and plucking, hardness and joint spacing. *Geomorphology* **130**, 374–383. doi: 10.1016/j.geomorph.2011.04.022

Krabbendam M and Hall AM (2019) Subglacial Block Removal: A Preliminary Analysis of Driving and Resisting Forces Under Different Glaciological Scenarios. SKB Report TR-19-18, Svensk Kärnbränslehantering AB.

Krabbendam M, Hall AM, Palamakumbura RN and Finlayson A (2022) Glaciotectonic disintegration of roches moutonnées in east Sweden: a transient phase during glacial ripping. *Geografiska Annaler: Series A, Physical Geography* **104**(1), 35–56. doi: 10.1080/04353676.2021.2022356

Krabbendam M, Palamakumbura R, Arnhardt C and Hall A (2021) Rock fracturing by subglacial hydraulic jacking in basement rocks, eastern Sweden: the role of beam failure. *GFF* **143**(4), 390–405. doi: 10.1080/11035897.2021.1939776

Leijon B (2005) Forsmark site investigation: Investigations of superficial fracturing and block displacements at drill site 5. SKB Report P-05-199, Svensk Kärnbränslehantering AB.

Leith D (1987) Drag on nonspherical objects. *Aerosol Science and Technology* **6**(2), 153–161. doi: 10.1080/02786828708959128

Lindbäck K and Pettersson R (2015) Spectral roughness and glacial erosion of a land-terminating section of the Greenland ice sheet. *Geomorphology* **238**, 149–159. doi: 10.1016/j.geomorph.2015.02.027

Loth E (2008) Drag of non-spherical solid particles of regular and irregular shape. *Powder Technology* **182**(3), 342–353. doi: 10.1016/j.powtec.2007.06.001

Lundqvist J (1987) Glaciodynamics of the Younger Dryas marginal zone in Scandinavia: implications of a revised glaciation model. *Geografiska Annaler: Series A, Physical Geography* **69**(2), 305–319. doi: 10.1080/04353676.1987.11880217

Lüthi M, Funk M, Iken A, Gogineni S and Truffer M (2002) Mechanisms of fast flow in Jakobshavn Isbræ, West Greenland: part III. Measurements of ice deformation, temperature and cross-borehole conductivity in boreholes to the bedrock. *Journal of Glaciology* **48**(162), 369–385. doi: 10.3189/172756502781831322

MacGregor JA and 9 others (2016) A synthesis of the basal thermal state of the Greenland ice sheet. *Journal of Geophysical Research: Earth Surface* **121** (7), 1328–1350. doi: 10.1002/2015JF003803

McCarthy C, Savage H and Nettles M (2017) Temperature dependence of ice-on-rock friction at realistic glacier conditions. *Philosophical Transactions of the Royal Society, A: Mathematical, Physical and Engineering Sciences* **375**(2086), 20150348. doi: 10.1098/rsta.2015.0348

https://doi.org/10.1017/jog.2022.49 Published online by Cambridge University Press

Morgan VI (1991) High-temperature ice creep tests. *Cold Regions Science and Technology* **19**(3), 295–300. doi: 10.1016/0165-232X(91)90044-H

Näslund JO, Rodhe L, Fastook JL and Holmlund P (2003) New ways of studying ice sheet flow directions and glacial erosion by computer modelling – examples from Fennoscandia. *Quaternary Science Reviews* **22**(2–4), 245–258. doi: 10.1016/S0277-3791(02)00079-3

Neupane B, Panthi KK and Vereide K (2020) Effect of power plant operation on pore pressure in jointed rock mass of an unlined hydropower tunnel: an experimental study. *Rock Mechanics and Rock Engineering* **53**(7), 3073–3092. doi: 10.1007/s00603-020-02090-7

Nye JF (1970) Glacier sliding without cavitation in a linear viscous approximation. *Proceedings of the Royal Society of London, Series A. Mathematical and Physical Sciences* **315**(1522), 381–403. doi: 10.1098/rspa.1970.0050

Patton H and 9 others (2017) Deglaciation of the Eurasian ice sheet complex. *Quaternary Science Reviews* **169**, 148–172. doi: 10.1016/j.quascirev.2017.05.019

Pless JC and 5 others (2015) 3D Characterization of fracture systems using terrestrial laser scanning: an example from the Lewisian basement of NW Scotland. *Geological Society, London, Special Publications* **421**(1), 125–141. doi: 10.1144/SP421.14

Quiquet A, Colleoni F and Masina S (2016) Long-term safety of a planned geological repository for spent nuclear fuel in Forsmark, Sweden and Olkiluoto, Finland. SKB Report TR-16-02, Svensk Kärnbränslehantering AB.

Ramana YV and Gogte BS (1989) Dependence of coefficient of sliding friction in rocks on lithology and mineral characteristics. *Engineering Geology* **26**(3), 271–279. doi: 10.1016/0013-7952(89)90014-8

Roberts DH and Long AJ (2005) Streamlined bedrock terrain and fast ice flow, Jakobshavns Isbrae, West Greenland: implications for ice stream and ice sheet dynamics. *Boreas* **34**(1), 25–42. doi: 10.1111/j.1502-3885.2005.tb01002.x

Ryser C and 7 others (2014) Sustained high basal motion of the Greenland ice sheet revealed by borehole deformation. *Journal of Glaciology* **60**(222), 647–660. doi: 10.3189/2014JoG13J196

Schweizer J and Iken A (1992) The role of bed separation and friction in sliding over an undeformable bed. *Journal of Glaciology* **38**(128), 77–92. doi: 10.3189/S0022143000009618

Shang J, Hencher SR and West LJ (2016) Tensile strength of geological discontinuities including incipient bedding, rock joints and mineral veins. *Rock Mechanics and Rock Engineering* **49**(11), 4213–4225. doi: 10.1007/s00603-016-1041-x

Singh PK and 5 others (2017) Indirect estimation of compressive and shear strength from simple index tests. *Engineering with Computers* **33**(1), 1–11. doi: 10.1007/s00366-016-0451-4

Sohlenius G, Hedenström A and Rudmark L (2004) Forsmark Site Investigation: Mapping of Unconsolidated Quaternary Deposits 2002-2003: Map Description. SKB Report R-04-39, Svensk Kärnbränslehantering AB.

Stokes GG (1951) On the effect of the inertial friction of fluids on the motions of pendulums. *Transactions of the Cambridge Philosophical Society* **9**, 1851.

Stroeven AP and 9 others (2016) Deglaciation of Fennoscandia. *Quaternary Science Reviews* **147**, 91–121. doi: 10.1016/j.quascirev.2015.09.016

Strömberg B (1989) *Late Weichselian deglaciation and clay varve chronology in east-central Sweden*. Sveriges Geologiska Undersökning, Serie Ca **73**, pp. 1–70.

Talbot CJ and Sirat M (2001) Stress control of hydraulic conductivity in fracture-saturated Swedish bedrock. *Engineering Geology* **61**(2-3), 145–153. doi: 10.1016/S0013-7952(01)00047-3

Witherspoon PA, Wang JS, Iwai K and Gale JE (1980) Validity of cubic law for fluid flow in a deformable rock fracture. *Water Resources Research* **16**(6), 1016–1024. doi: 10.1029/WR016i006p01016

Wright PJ, Harper JT, Humphrey NF and Meierbachtol TW (2016) Measured basal water pressure variability of the western Greenland ice sheet: implications for hydraulic potential. *Journal of Geophysical Research: Earth Surface* **121**(6), 1134–1147. doi: 10.1002/2016JF003819

https://doi.org/10.1017/jog.2022.49 Published online by Cambridge University Press